Geomorphological signatures of known hurricanes and validation of theoretical emplacement formulations: Coastal boulder deposits on Cuban low-lying marine terraces

Pedro Dunán-Avila, Christine Authemayou, Marion Jaud, Kevin Pedoja, Julius Jara-Muñoz, Stephane Bertin, Leandro Peñalver-Hernández, France Floc'H, Arelis Nuñez-Labañino, Patricio Winckler, et al.

Marine Geology 480 (2025) 107438

Contents lists available at ScienceDirect

Marine Geology

journal homepage: www.elsevier.com/locate/margo

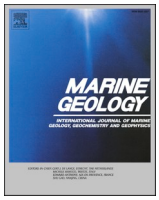

Research Article

Geomorphological signatures of known hurricanes and validation of theoretical emplacement formulations: Coastal boulder deposits on Cuban low-lying marine terraces

Pedro Dunán-Avila [a,*], Christine Authemayou [a], Marion Jaud [a,b], Kevin Pedoja [c], Julius Jara-Muñoz [d], Stephane Bertin [a], Leandro Peñalver-Hernández [e], France Floc'h [a], Arelis Nuñez-Labañino [e], Patricio Winckler [f,g,h], Jean Pierre-Toledo [i], Pedro Benítez-Frometa [e], Hassan Ross-Cabrera [e], Pauline Letortu [j], Angel Raúl Rodríguez-Valdés [k], Noel Coutín-Lobaina [l], Denovan Chauveau [a]

[a] Université de Brest, Geo-Ocean, CNRS, Ifremer, UMR6538, F-29280 Plouzané, France
[b] Université de Brest, Pôle Image et Instrumentation - IUEM, CNRS, IRD, UAR 3113, F-29280 Plouzané, France
[c] Université de Caen Normandie, Laboratoire Morphodynamique Continentale et Côtière, CNRS, Caen, France
[d] Hochschule Biberach, Faculty of Civil Engineering, Karlstraße 11, Biberach an der Riß, Germany
[e] Instituto de Geología y Paleontología, Servicio Geológico de Cuba, La Habana, Cuba
[f] Universidad de Valparaíso, Escuela de Ingeniería Oceánica, Valparaíso, Chile
[g] National Research Center for Integrated Natural Disaster Management (CIGIDEN), Santiago, Chile
[h] Centro de Observación Marino para Estudios de Riesgos del Ambiente Costero (COSTAR), Valparaíso, Chile
[i] Escuela de Ciencias del Mar, Facultad de Ciencias del Mar y Geografía, Pontificia Universidad Católica de Valparaíso, Valparaíso, Chile
[j] Université de Brest, CNRS, LETG UMR 6554, F-29280 Plouzané, France
[k] Centro de Servicios Ambientales, Sancti Spíritus, Cuba
[l] Centro de Servicios Ambientales, Parque Nacional "Alejandro de Humboldt", Baracoa, Guantánamo, Cuba

ARTICLE INFO

Editor: Shu Gao

Keywords:
Coastal boulder deposits
Hydrodynamic equations
Minimum flow velocity
Maximum orbital velocity
Structure from-motion-photogrammetry

ABSTRACT

Coastal boulder deposits, observed worldwide, provide geomorphological evidence of extreme wave events such as storms, hurricanes and tsunamis. Theoretical formulations have been developed for determining hydrodynamic conditions responsible for boulder emplacement on the shore, which increasingly make use of boulder geometry and associated site geomorphology. Nevertheless, information on extreme events responsible for the emplacement of coastal boulders is rarely available, meaning there has been limited opportunity to test existing formulations in the light of real hydrodynamic and geomorphic data. In this study, we take advantage of the important record of coastal boulder deposits on Cuba Island to compare the hydrodynamic parameters (minimum flow velocity) deduced from the boulders' morphology and emplacement characteristics, with hydrodynamic conditions (maximum wave height and orbital velocity) that occurred during the tropical cyclones responsible for the boulders' actual emplacement. We selected four sites where three hurricanes have emplaced five boulders on low-lying coral reef terraces over the last 50 years. Using terrestrial Structure-from-Motion photogrammetry, we determined with precision the boulders' shape and volume, which in combination with density, mode of emplacement and distance from the shore, were used to calculate the minimum flow velocity responsible for dislocation of the coral reef terrace and inland transport. To serve as comparisons, available modelled data of wave height and period were used to estimate the maximum orbital velocity that possibly occurred during the weather event using linear wave theory. Our results show that for all boulders studied except one, there is a good agreement between the values of minimum flow and maximal orbital velocities, with minimum flow velocities for boulder emplacement consistently smaller than the maximum wave orbital velocity during the weather event. The difference observed for one boulder is attributed to specific site effects, highlighting in this case the limitation of using distant hydrometeorological data for characterizing wave processes responsible for coastal boulder deposits. Helped by detailed data collected on boulders with large differences in morphology including

* Corresponding author.
E-mail address: pdunanavila@gmail.com (P. Dunán-Avila).

https://doi.org/10.1016/j.margeo.2024.107438
Received 4 July 2024; Received in revised form 12 November 2024; Accepted 16 November 2024
Available online 22 November 2024

size, and mode of emplacement, this study confirms the pertinence of using formulations relating boulder morphology and site characteristics to the minimum flow velocity that detached and transported the boulder. It further emphasizes the importance of obtaining adequate boulder and geomorphic setting characterizations to link geomorphological proxies and extreme wave events.

1. Introduction

Coastal boulder deposits (CBDs) are some of the most striking geomorphic evidence of extreme coastal flooding (Williams and Hall, 2004; Scicchitano et al., 2007; Goto et al., 2010; Terry et al., 2013) and as such they are commonly used to infer the magnitude of marine inundation events over long timescales (Etienne et al., 2011; Engel and May, 2012). CBDs have been studied in many coastal areas worldwide (e.g., Noormets et al., 2004; Hall et al., 2006; Salzmann and Green, 2012; Yu et al., 2012; Araoka et al., 2013; Shah-Hosseini et al., 2016; Terry et al., 2016; Pedoja et al., 2023; Bourman et al., 2023) and are considered significant geomorphological features in coastal hazard analysis (e.g., Moore and Moore, 1984; Mastronuzzi and Sansò, 2000; Kelletat and Schellmann, 2002; Rubin et al., 2000; Scheffers and Kelletat, 2003; Matsukura et al., 2007; Hansom et al., 2008; Frohlich et al., 2009; Goto et al., 2009; Bourgeois and Mac Innes, 2010; May et al., 2010; Regnauld et al., 2010; Paris et al., 2011; May et al., 2015).

Since the seminal work of Young et al. (1996) and Nott (1997, 2003a, 2003b) theoretical equations based on the boulder morphology have been proposed to estimate the required wave height to initiate boulder movement. In addition, several studies used the Nott's equations to determine the origin, either storm or tsunami, of boulders emplacement (e.g., Scheffers and Kelletat, 2006; Bryant and Haslett, 2007; Mastronuzzi et al., 2007; Scheffers et al., 2008). However, using these equations, large boulders tend to be inaccurately associated with tsunami waves while small boulders are usually associated with storm waves (e.g., Morton et al., 2006, 2008; Kelletat, 2008; Paris et al., 2010; Switzer and Burston, 2010). As a result, the hydrodynamical equations of Nott's have been improved through time (e.g., Pignatelli et al., 2009; Barbano et al., 2010; Benner et al., 2010; Nandasena et al., 2011a, 2011b; Mottershead et al., 2014; Gandhi et al., 2017), but their pertinence for CBDs analysis is still matter of discussion in the scientific literature (e.g., Cox et al., 2018, 2020; Scicchitano et al., 2020, 2021; Nandasena et al., 2022). Indeed, when early work focused on wave height estimates, recent studies suggest estimating the minimum flow velocity required for boulder entrainment, hence refraining from estimating the resulting wave heights during the event (Nandasena et al., 2013, 2022) due to a lack of empirical research on the wave heights responsible for the siting of the boulders.

Using novel hydrodynamic equations of incipient motion, precise determination of boulder metrics such as volume, density, mass, distance from the coast, and elevation, has been shown critical to infer the mode of emplacement and obtaining reliable results on the minimum flow velocity. Boulder volume estimation can be realized in different ways. Some studies estimated volume by measuring the three maximum boulder axes, with results more or less precise depending on boulder geometry (Suanez et al., 2009; Barbano et al., 2010; Pepe et al., 2018; Khalfaoui et al., 2024), while other studies use close-range remote-sensing techniques such as terrestrial laser scanning (Schneider et al., 2019) and photogrammetry (e.g., Boulton and Whitworth, 2018; Nagle-McNaughton and Cox, 2019; Boesl et al., 2020; Sedrati et al., 2022; Pedoja et al., 2023). Volume estimation with remote sensing and photogrammetry, although highly precise, involve a significant financial cost. It is still questionable, however, to what extent the precise determination of boulder volume is fundamental for inferring the hydrodynamic conditions responsible for boulder emplacement. We believe the main reason is the scarcity of geomorphic and wave data for assessing boulder emplacement conditions.

Here, we present, the analysis of five boulders emplaced by three recent hurricanes along the Cuban Archipelago (Fig. 1), where CBDs are named *huracanolitos* (e.g., Iturralde-Vinent, 2017; Pedoja et al., 2023). More specifically, we focused on reconciling theoretical approaches using boulder morphology and its geomorphic setting with the hydrodynamic conditions that caused the emplacement of the boulders. In order to estimate the volume of CBDs, we adapted a structure-from-motion (SfM) photogrammetry workflow. Using the most recent hydrodynamic equations, we then calculated the minimum flow velocity responsible for the boulder's inland transport. To quantitatively assess the pertinence of these equations, and to evaluate the impact of boulders' volume on the results, we compared the calculated minimum flow velocity with the maximum orbital velocities that occurred during recent associated hurricanes based on archived data models using WAVEWATCH III® and linear wave theory.

2. Settings

2.1. Geodynamic and hydrodynamic setting of Cuba Archipelago

The archipelago of Cuba is located on the North American plate at its southern boundary with the Caribbean plate (Cotilla Rodríguez, 2011; Corbeau et al., 2017; Fig. 1). Along this EW-trending plate boundary consisting of the *Septentrional Oriente* Fault Zone and the Enriquillo Plantain-Garden Fault Zone, the North American plate moves westward (70–80°N) at a rate of 18–20 ± 3 mm.yr^{-1} (DeMets et al., 2000; Mann et al., 2002; Calais et al., 2016). The *Septentrional Oriente* Fault Zone is most seismic on the island of Cuba and is a potential tsunami generator (e.g., there is evidence of major earthquakes ranging from 5.0 to 7.2 Mw between 1766 and 2020; Cotilla Rodríguez, 2014; Authemayou et al., 2023; Calais et al., 2023).

Wave climatology in Cuba is influenced by a complex combination of meteorological, oceanographic and geographical factors and is poorly documented in the literature. Seasonal effects, local weather conditions, coastal bathymetry and extreme weather events are all factors to be considered to describe wave climatology in Cuba. On the Cuban island, tides are mixed and semi-diurnal, with a mean amplitude of 0.5 m (i.e., microtidal). Tidal currents are relatively weak around the island (up to 0.5 kn), except at the entrance of bays and ports, where they can reach speeds of 2 to 4 kn. Modal waves are also generally weak (annual mean significant wave height is <1.0 m; Reguero et al., 2013). However, wave height can reach considerable values during the arrival of a cold fronts or tropical cyclones through the region (Servicio Hidrográfico y Geodésico de la República de Cuba, 2003). The most important climate changes on this coast are linked to the presence of disturbances in the tropical circulation, causing the arrival of ocean waves from the east and tropical storms (INSMET, 2024).

2.2. Tropical cyclones in Cuba island

Tropical cyclones (e.g., tropical depressions, tropical storms and hurricanes) affect the Cuban archipelago annually from June 1st to November 30th during Cuba's cyclonic season, but cyclone occurrence outside this period have been also documented (Roura-Pérez et al., 2018; Fernández-Alvarez et al., 2020). The genesis of tropical cyclones in the North Atlantic area is divided into six regions, and Cuba experiences cyclones coming from all these regions (Roura-Pérez et al., 2018). These events are classified internationally according to maximum wind and minimum pressure, resulting in the hurricane category (Simpson, 1974). According to NOAA (2022a, 2022b), 86 hurricanes made landfall

on the island of Cuba between 1851 and 2021 (Appendix A). During this period, 59 hurricanes with category ≥3 occurred, 32 of which were category 4 and 5 hurricanes. These events can produce larger waves and wave breaking closer to the shore than typical coastal storms (Raichlen, 2012).

The five CBDs studied here were deposited by three recent hurricanes according to local records, verbal witnesses, photographic evidence, satellite image analyses and past studies: Hurricane Lili in 2002 (category 4) that passed through the Cienfuegos area with category 1 and emplaced the two boulders at site Faro Colorado 1 and Faro Colorado 2; the 1935 Cuba Hurricane (category 4) that passed through the Cienfuegos and Sancti Spíritus area with category 3 for the boulder at El Capitan; and Hurricane Matthew in 2016 (category 5) that passed through the Guantánamo area with category 4 for the boulders at Bate Bate and Bahia de Boma sites (Fig. 1). We here with provide a brief description of the three hurricanes.

2.2.1. The 1935 Cuba Hurricane

The 1935 Cuba Hurricane was an intense and destructive tropical cyclone that caused damage in Cuba in September 1935 (Figs. 1 and 2A). Information about this hydro-meteorological event is the most limited due to poor equipment availability at the time. The storm formed from a tropical depression in the center of the Caribbean Sea on September 23. On September 28, the storm reached major hurricane intensity before landing on Cuba near Cienfuegos, at 08:00 UTC, as a category 3 hurricane. The large storm surge destroyed low-lying coastal towns, especially in Cienfuegos province. In Trinidad and Sancti Spíritus regions, buildings were completely swept away. The hurricane crossed Cuba with minimal intensity change before reentering the Atlantic Ocean on September 28. After passing over Cuba, the hurricane intensified and became category 4. The tide is reported to have risen 4.5 m above normal at Bimini (Bahamas) destroying nearly half of the island due to the extreme storm surge (McDonald, 1935).

2.2.2. Hurricane Lili in 2002

Hurricane Lili was a category 4 hurricane originated as a tropical wave that moved over the tropical Atlantic Ocean from the western coast of Africa (Figs. 1 and 2B). Resuming its west-northwest trajectory, Lili became a hurricane on 30 September as it passed over Little Cayman and Cayman Brac. Lili continued to strengthen and, its winds were near 179 km/h when the center moved over the southwestern tip of the Isla de la Juventud on the morning of 1 October and over western mainland Cuba a few hours later. The eye of hurricane Lili passed ~183 km south of the Cienfuegos province as a category 1 hurricane, gaining in organization and intensity. Along the Cienfuegos coastline, the hurricane produced a significant wave height of 2.4 m and associated peak wave

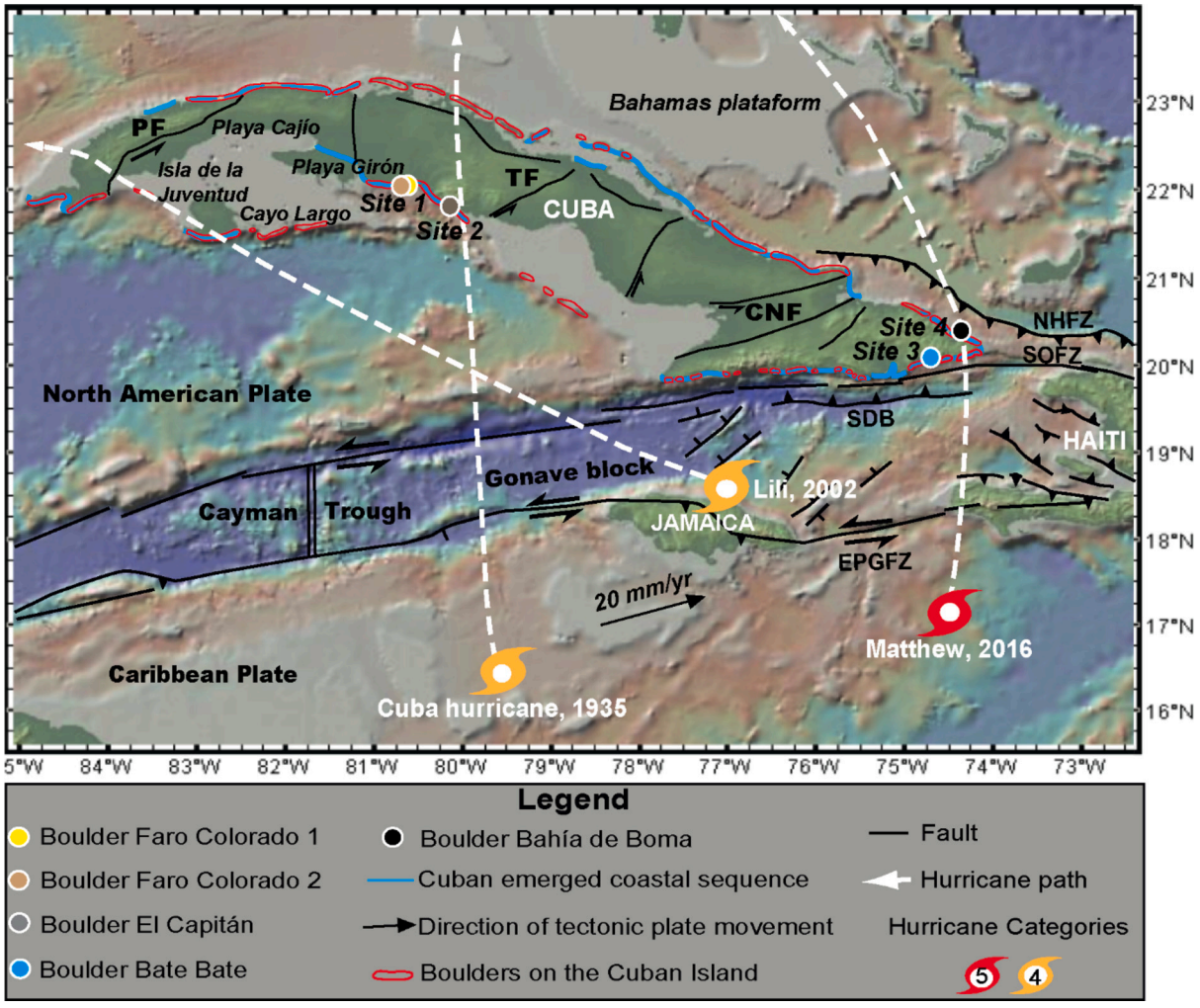

Fig. 1. Geodynamics of Cuba archipelago and locations of the studied coastal boulders. The paths and categories of the hurricanes that produced the studied boulder's emplacement are indicated. Spatial distribution of boulders on the Cuban Island is from Matos-Pupo et al. (2023). Marine terrace sequences have been drawn according to Peñalver et al. (2021). Faults of Cuba island are indicated according to Iturralde-Vinent et al. (2016). PF: Pinar fault, TF: la Trocha Fault, CNF: Cauto Nipe Fault, NHFZ: North Hispaniola Fault Zone, SOFZ: *Septentrional Oriente* Fault Zone; EPGFZ: Enriquillo Plantain-Garden Fault Zone; SDB: Santiago Deformed Belt.

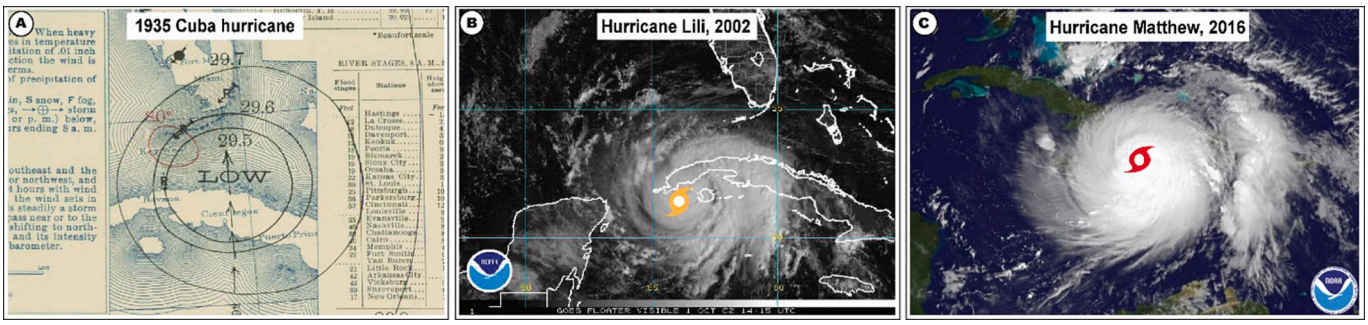

Fig. 2. Hurricanes that emplaced the studied Cuban CBDs. (A) Surface weather analysis of the 1935 Cuba Hurricane in the Florida Straits on September 28, 1935. (B) Hurricane Lili satellite image over Cuba on October 1, 2002. (C) Hurricane Matthew image from NOAA's GOES-East satellite at 7:45 a.m. EDT on October 4, 2016, within the hour of landfall in western Haiti. Credits from NOAA Digital Central Library (A, B) and NASA/NOAA GOES Project (C).

period of 8.8 s according to Archived Data WAVEWATCH III® Production Hindcast (NOAA Environmental Modeling Center, 2023; Fig. 3A). The hurricane had a storm surge of 2.0–4.0 m in Louisiana (National Weather Service Forecast Office, 2002). Tide gauges at Crewboat Canal near Calumet and Vermillion Bay measured a storm tide water height of 3.7 m and 3.5 m, respectively (Pasch et al., 2004; Lawrence, 2011).

2.2.3. *Hurricane Matthew in 2016*

Formed as a tropical wave on 23 September 2016, category 5 Hurricane Matthew moved westward across the tropical Atlantic Ocean at speeds from 37 to 46 km/h over the next three days (Figs. 1 and 2C, D). The eye made landfall on the eastern tip of Cuba, near Juaco, as a major hurricane (category 4) on 5 October 2016. Cuba's Institute of Meteorology reported a storm surge of 3.0 m – 4.0 m along the southern coast of Guantánamo province, affecting the towns of Imías, San Antonio de Sur and Maisí (Stewart, 2017). According to WAVEWATCH III® Production Hindcast, the hurricane produced a significant wave height of 7.3 m with a period of 11.7 s and a storm surge of 3.0 m - 4.0 m in Bate Bate region (Fig. 3B; NOAA Environmental Modeling Center, 2023). Along the northern coastline of the Guantánamo province, storm surge exceeded 3.5 m along with waves of 4.5 m – 6.0 m high (Stewart, 2017). On the north coast, specifically in the Baracoa region (Bahia de Boma site), it produced a significant wave height of 7.4 m with a peak period of 10.7 s and a storm surge of 3.0 m - 4.0 m (Fig. 3C; NOAA Environmental Modeling Center, 2023).

2.3. *Coastal boulder deposits on the Cuban lower coral reef terraces*

Cuban coastal boulders are most generally torn from the offshore platform or sea cliff during extreme wave events and thrown inland (e.g., Iturralde-Vinent, 2017; Matos-Pupo et al., 2023; Fig. 1). Commonly named *huracanolitos* in Cuba (e.g., Núñez Jiménez, 1973; Iturralde-Vinent, 2017; Beltrán-Fonseca, 2019; Aguirre Feria et al., 2021; Pedoja et al., 2023), they are mostly located on the lower Pleistocene marine and coral reef terraces (Iturralde-Vinent, 2017). The associated unsorted debris ridges, are known as *Camellones de Tormentas* (Peñalver et al., 2008; Peñalver Hernández et al., 2009). These consist of fine to medium-grained sand of carbonate composition containing blocks of limestone and corals of *Jaimanitas* Fm. and are frequently placed far from the inland cliffs by waves.

The first studies of *huracanolitos* in Cuba were carried out by Núñez Jiménez (1959, 1982). Recently, Cuban coastal boulder fields and unsorted debris ridges were studied, near la Havana (Rojas-Consuegra and Isaac-Mengana, 2007; Rojas-Consuegra and Isaac-Mengana, 2008; Rojas-Consuegra et al., 2019), near Trinidad (Rodríguez-Valdés and Acosta-Rodríguez, 2017; León-Brito et al., 2021), in Jardines de la Reina Archipelago (Matos-Pupo et al., 2018), near Guantanamo Bay (Magaz and Portela, 2017; Beltrán-Fonseca, 2019) and in Santiago Province, where a coastal boulder of 210 tons was reported (Pedoja et al., 2023).

The largest CBDs reported are found on the southern coast of the main island (Iturralde-Vinent, 2017; Pedoja et al., 2023). This preferential location may be related either to the dominant tectonic activity in this area and its potential tsunamic sources, or because this coastal stretch is also the most directly impacted by hurricanes (Fig. 1).

3. Methods

In order to study the transport and emplacement of the selected CBDs, we first analyzed the morphology of the studied site and the boulder geometry. Specifically, we determined the volume of the boulders using Structure-from-Motion (SfM) photogrammetry and their density using the water immersion method on samples. These metrics were used to calculate the minimum flow velocity required for the emplacement of the CBDs using the hydrodynamic equations of Nandasena et al. (2022). Evaluating the results obtained was performed by taking the maximum wave orbital velocity that occurred at the studied

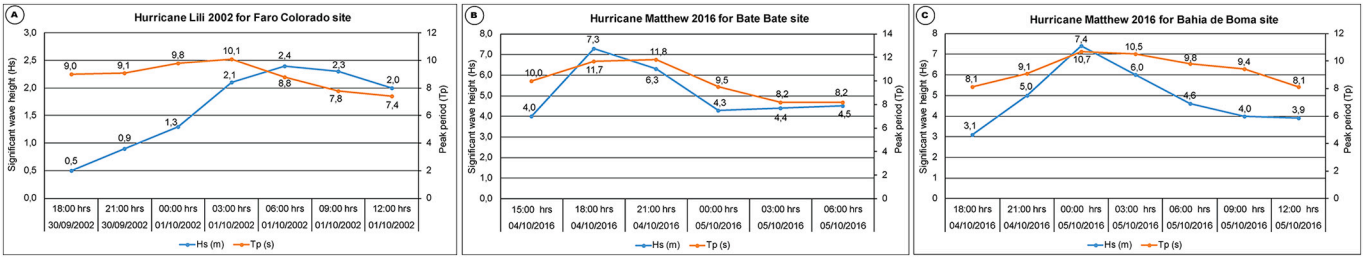

Fig. 3. Wave characteristics (Hs is significant wave height and Tp is peak period) of the hurricanes studied for the study area according to Archived Data WAVEWATCH III® Production Hindcast (NOAA Environmental Modeling Center, 2023). Wave data for (A) Hurricane Lili in 2002 in the Cienfuegos coastline (22°00′00.0"N 80°30′00.0"W); (B) Hurricane Matthew in 2016 in the Bate Bate coastline (20°00′00.0"N 74°30′00.0"W); and (C) Hurricane Matthew in 2016 in the Baracoa coastline (20°30′00.0"N 74°30′00.0"W). Geographic coordinates are provided in WGS84 and correspond to the specific locations where wave measurements were taken.

Table 1
Photogrammetry error and target point of the boulders studied in Cuba Island.

ID Boulder	Coordinates		Number of photos	Photos aligned (%)	Total points in the cloud	Average point density (pt/cm^2)	Number of reconstruted points on targets							Total number of reconstruted points on targets	Total error of control scale bars (cm)	Mean error (cm)	Standard deviation error	RMSE
	Latitude	Longitude					Ruler 1	Ruler 2	Ball 1	Ball 2	Ball 3	Ball 4	Ball 5	Ball 6				
Faro Colorado 1	22.033317	−80.442867	1419	100	184,337,725	435	767,990	725,785	12,080	11,540	13,210	15,021	11,254	11,541	1,568,421	4.351	0.977	4.379	4.487
Faro Colorado 2	22.033684	−80.442675	326	100	17,938,051	185	142,598	233,602	3821	3997	4552	2460	3997	4352	399,379	0.365	0.232	0.292	0.372
El Capitan	21.789483	−80.034883	2766	100	133,114,888	347	711,245	768,524	124,101	10,945	12,212	15,435	11,254	11,710	1,665,426	0.185	0.121	0.144	0.189
Bate Bate	20.009433	−74.870500	1938	100	86,155,509	209	154,798	254,685	4785	5875	4651	3512	4510	3541	436,357	0.237	0.163	0.177	0.241
Bahia de Boma	20.340536	−74.444385	1315	100	179,653,492	397	745,285	739,442	11,433	14,240	11,427	14,053	11,293	10,531	1,557,704	0.242	0.067	0.243	0.252

site during the responsible wave event as an upper bound, which was derived from application of the linear wave theory to hindcasted wave time series at selected nodes (WAVEWATCH-III model data) and depth-information provided by bathymetric surveys.

3.1. Morphological analysis of the studied sites

The morphological analysis of the coastal area and boulder setting included topo-bathymetric surveys and detailed descriptions of the boulder characteristics. Geomorphological characterization involved the identification of the substrate of the boulders, the presence of fossil corals heads in normal or inverted growth position and the surface rugosity of the boulder. Satellite images (Landsat and WorldView) were interpreted to analyze the study area before and after the hurricane's passage. The topographic and bathymetric data were acquired using a real-time kinematic differential Global Positioning System (RTK DGPS model Topcon HiPer V) onshore and a Deeper Smart sonar Pro+2 (Deepersonar, 2024) offshore.

3.2. Boulder characteristics: SfM photogrammetry, volume and density determination

To generate a 3D-scaled SfM point cloud of each studied boulder, we adapted an easy SfM workflow using Agisoft Metashape software (version 1.7.2). We surveyed each CBD obtaining pictures between 0.5 m - 3 m distance from the boulder and also climbing on the boulder to maximize the diversity of picture angles. The survey was carried over a time-lapse of ~30 min and under cloudy conditions to avoid shadows created by direct sunlight (Gienko and Terry, 2014). A 12 megapixels, Panasonic Lumix DMC GM5, with a focal length of 12 mm, 4592 × 2584 resolution image and a pixel size of 3.79 × 3.79 μm, was used to capture pictures.

For scaling SfM results and assessing the quality of measurements, we used six wooden balls as photogrammetric targets (Table 1) as in Pedoja et al. (2023). The diameter of the balls is $30 \pm 0.2 \times 10^{-3}$ m, as verified by repeated caliper measurements. We complemented these targets with two 70 × 10 cm wooden scales (Table 1). All these targets were used as reference scale bars to correct the spherical distortion inherent to the camera optics and perform an auto-calibration. We further used these targets to check possible distortion after post-processing and the generation of the resulting 3D model. In order to create a point cloud and a solid volume, we followed the software workflow: we first aligned the images to identify tiepoints, which were then used in bundle adjustment to compute the 3D dense clouds in a second step (Table 1). Following the method of James et al. (2019) we determined the total error of the point cloud on control scale bars, and reported the mean, standard deviation of error and the RMSE (Table 1) as measurement quality metrics. Finally, the dense point cloud was converted to a 3D solid using the software Cloud-Compare®. To account for uncertainties in the resulting 3D solid (e.g., due to the point cloud density), we conducted a sensitivity test by resampling point clouds using different values of minimum distance between points, followed by point cloud meshing and volume estimation.

The 3D model was used to determine the morphology and morphometric characteristics of the boulders. The boulder dimensions were determined by projecting the 3D model onto 2D sections. We measured the surface area of each projected section "ab", "ac" and "bc" planes using MeshLab (Fig. 4), where a, b and c are the length of the boulder axes for the maximum, intermediate and minimum axis, respectively. These were used to estimate the virtual coefficients and wave-induced flow velocities (section 3.3) in the equations of Nandasena et al. (2022). To estimate the mass of the boulder, we first estimated the density of boulder samples using the water immersion method (e.g., Pepe et al., 2018). Measurements were repeated three times to obtain an average density value. For the Bate Bate boulder, we used a density of 2.59 g/cm^3, which was determined by Beltrán-Fonseca (2019; Table 2).

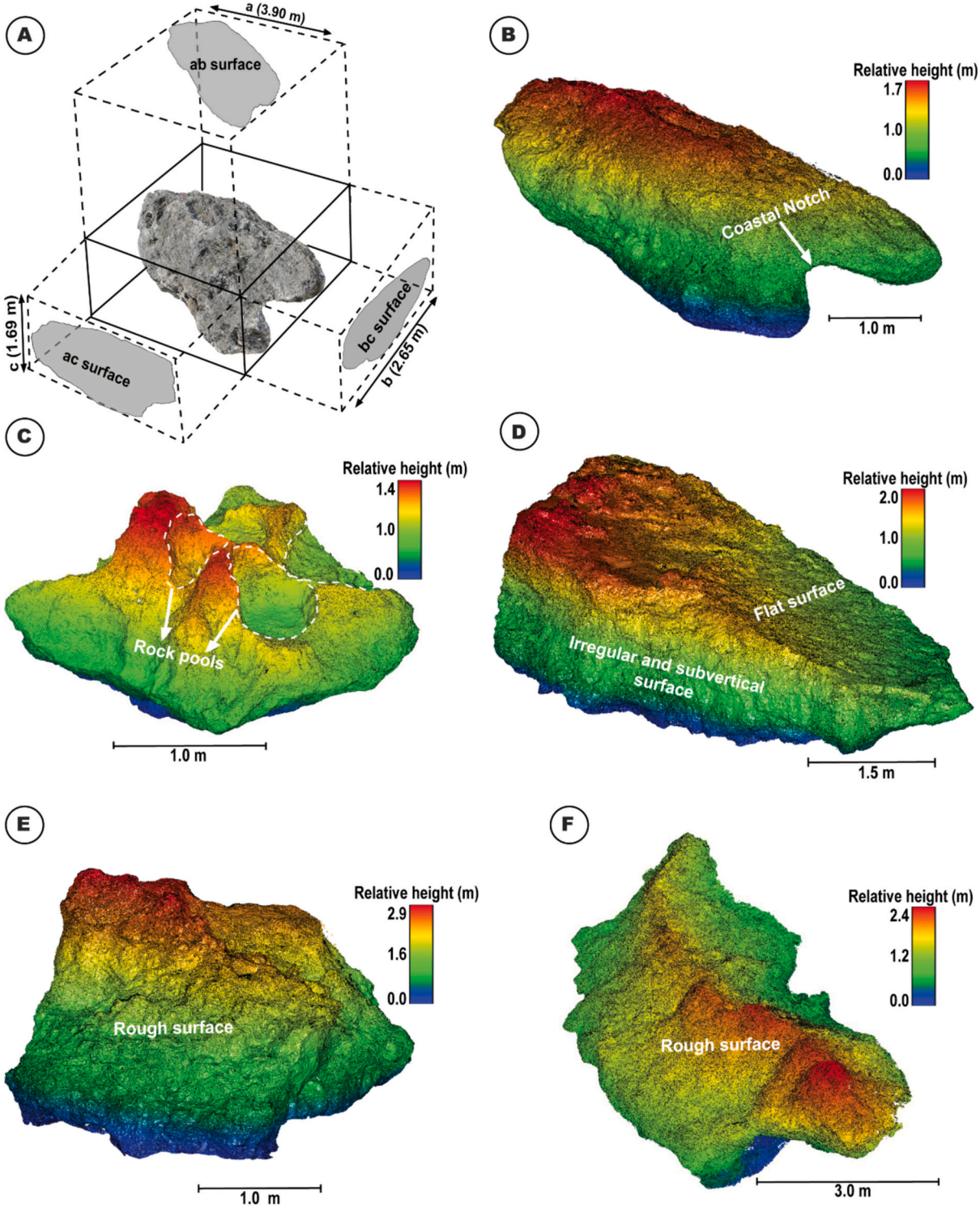

Fig. 4. (A) Polygonal model of the Faro Colorado 1 CBD; dimensional features are shown: a - b - c axis lengths and ab-ac-bc projected surfaces. Perspective view of the CBDs highlighting relative elevation and surfaces: (B) Faro Colorado 1 boulder, (C) Faro Colorado 2 boulder, (D) Bate Bate boulder, (E) El Capitan boulder and (F) Bahia de Boma boulder.

3.3. Minimum flow velocity for boulder emplacement

The metrics estimated for the CBDs (see above), were used to calculate the minimum flow velocity responsible for the boulder emplacement using the hydrodynamic equations of Nandasena et al. (2022). The energy transmission from the impacting waves to the boulder has been conceptualized with different mathematical relationships describing the whole transport process through three stages: a) incipient motion (Nott, 2003b), b), transport (Imamura et al., 2008), and c) deposition (Goto et al., 2009).

Nandasena et al. (2011a, 2013, 2020, 2022) developed a model to calculate the flow velocity needed to initiate the movement of a boulder for different settings (sliding, overturning, saltation/lifting) and boulder preconditions, namely submerged/subaerial (SB/SA), joint-bounded

Table 2
Location, size, and pre-transport setting of the boulders. Comparing boulder masses based on field measurements (a*b*c) with those computed using Structure-from Motion photogrammetry (SfM). Rock dimensions (a, b, c) are given to the nearest 5 cm.

ID Boulder	Pre-setting scenario	Type of movement	Axis length (m)			a-Axis Direction	Distance to coastline (m asl)	Elevation (m asl)	Volume SfM (m^3)	Volume a*b*c (m^3)	Average density (g/cm^3)	Mass based on SfM (tons)	Mass based on a*b*c (tons)	Difference between masses (%)
			a	b	c									
Faro Colorado 1	Cliff-edge boulder	Overturning	3.90	2.65	1.69	24°	68.5 ± 1.0	6.0 ± 1.0	8.7 ± 1.6	17.47	2.40	20.88 ± 3.8	41.92	100.76
Faro Colorado 2	Cliff-edge boulder	Overturning	2.39	2.33	1.39	151°	116 ± 1.0	7.2 ± 1.0	1.99 ± 0.3	7.74	2.40	4.77 ± 0.7	18.58	289.46
El Capitán	Joint-bounded boulder	Saltation/ lifting	6.10	3.90	2.85	167°	12.5 ± 1.0	1.2 ± 1.0	29.2 ± 3.1	67.80	2.56	74.75 ± 7.9	173.57	132.20
Bate Bate	Cliff-edge boulder	Overturning	7.46	3.85	1.95	153°	9.5 ± 1.0	6.0 ± 1.0	25.9 ± 2.6	56.01	2.59	67.08 ± 6.7	145.06	116.24
Bahia de Boma	Cliff-edge boulder	Overturning	9.66	4.41	2.36	350°	38.0 ± 1.0	5.8 ± 1.0	31.5 ± 2.5	100.5	2.37	74.65 ± 5.9	238.27	219.19

boulder (JBB), and cliff-edge boulder (CEB). Nandasena et al. (2022) integrated the real surface and the axes dimensions through a set of virtual coefficients. The authors considered the forces acting on boulders and their moments on a cubic/cuboid boulder such that the area of drag force Ad = ac, the area of lift force Al = ab and the volume of the boulder V = abc. In such a model, drag and lift forces act to move the boulder, reduced-gravity forces and friction forces resist when the waves impact the boulder. The equations considering the real surfaces along the boulder axes are defined as the virtual drag coefficient (C_{dv}), the virtual lift coefficient (C_{lv}) and the virtual volume coefficient (C_{vv}), so that:

$$\text{Virtual drag coefficient} : C_{dv} = \frac{A_d}{ac} C_d \tag{1}$$

$$\text{Virtual lift coefficient} : C_{lv} = \frac{A_l}{ab} C_l \tag{2}$$

$$\text{Virtual volume coefficient} : C_{vv} = \frac{V}{abc} \tag{3}$$

where A_d is the actual drag area, A_l is the actual lift area and V is the real volume of boulder.

These virtual coefficients model the actual volume and the projected area of the boulder (e.g., Fig. 4A). Also, they improve the accuracy of the forces in the incipient motion formulas (Nandasena et al., 2022). The equations for the different boulder settings and preconditions are as follows:

$$\text{Minimum flow considering rolling (CEB)} : u^2 = \frac{2C_{vv}\left(\frac{\rho_s}{\rho_w} - 1\right)gc}{C_{lv} - C_{dv}\left(\frac{c^2}{b^2}\right)} \tag{4}$$

$$\text{Minimum flow considering Saltation} \Big/ \text{lifting (CEB)} : u^2 = \frac{2C_{vv}\left(\frac{\rho_s}{\rho_w} - 1\right)gc}{C_{lv} - \mu_s C_{dv}\left(\frac{c}{b}\right)} \tag{5}$$

$$\text{Minimum flow velocity considering Lifting (JBB)} : u^2 \geq \frac{2C_{vv}\left(\frac{\rho_s}{\rho_w} - 1\right)gc(cos\theta + \mu_s sin\theta)}{C_{lv}} \tag{6}$$

Here, u is the minimum flow velocity, μ_s is the coefficient of static friction between boulder and substrate, g is the gravitational constant (taken as 9.81 m/s^2), C_d is the coefficient of drag, C_l is the coefficient of lift, ρ_b is the density of the boulder, ρ is the density of seawater (taken as 1.020 g/cm^3) and θ is the ground slope at the pre-transport location.

The coefficients of drag, lift and static friction contribute to the magnitude of the forces considered in the incipient movement formulas, and influence the minimum flow velocity and modes of boulder transport (Nandasena, 2020). The values of drag coefficient (C_d) described in the literature range from 1.0 to 2.5 (Noormets et al., 2004; Malavasi and Guadagnini, 2007; Imamura et al., 2008; Paris et al., 2010; Nandasena et al., 2011b; 2022). For the lift coefficient (C_l) Einstein and El-Samni (1949) adopted a value of 0.178. Research by Nandasena (2017) and Nandasena et al. (2022) reported C_l values ranging between 0.1 and 0.8. Rovere et al. (2017) calculated lift coefficient indirectly using the Nott's approach on two Bahamian boulders of 13 and 33 t, obtaining values of C_l ranging between 2 and 2.7. Pedoja et al. (2023) considered C_l values between 2 and 2.5 for a boulder of 210 tons on the South coast of Cuba. In this study, we considered a static friction coefficient of μ_s = 0.7 (Nandasena et al., 2011a, 2013, 2022; Rovere et al., 2017; Pedoja et al., 2023). To estimate minimum flow velocities, we used a range of drag

coefficients between 1.8 and 2.2 and lift coefficients between 1.8 and 2.7. This approach allowed us to present a range of plausible flow velocities, incorporating uncertainty. We generated probability density functions based on the results of the flow velocity equations using the specified ranges of lift and drag coefficients.

3.4. Maximum wave orbital velocity

Numerous coastal parameters including sediment mobility, transport and suspension, bed protection measures and fluid-structure interactions require estimating wave-induced orbital velocities. A simple method for this calculation uses linear wave theory to convert wave height and period into orbital velocity at specific water depths (Sleath, 1984). Herein, water depth at the initial boulder location was obtained using bathymetric data and interpretation of the boulder origin, either sea-cliff edge or offshore platform. Significant wave heights and peak periods during recent hurricanes in the studied areas were determined using the WAVEWATCH III® Production Hindcast from Marine Branch Archive (199907 – 200711) and NODC THREDDS (NODC Archive, 2005–2018) archived model data. For the 1935 Cuba Hurricane (category 3) in the region of Trinidad, because there are no instrumental records for this event, we had recourse to theoretical values of storm surge, wave height and period provided by NOAA Ocean Explorer (2013) for category 3 hurricanes. Although covering a large range, it led to using significant wave heights between 2 m and 8 m, wave periods from 10 s to 15 s and storm surge values from 2.7 m to 3.8 m. Given that this hurricane produced a storm tide (i.e., maximum water level) in the region of Bimini, Bahamas, of 4.5 m (McDonald, 1935), and the astronomical tide in this region is less than 1 m (NOAA Tide Predictions, 2023), the storm surge at this site could have been around 3.5 m; value which is in agreement with the range of values proposed by NOAA Ocean Explorer (2013) for category 3 hurricanes.

The use of linear wave theory to derive orbital velocities is supported experimentally by Kirkgöz (1986), who revealed a reasonable agreement between the theory and observed orbital velocities beneath wave crests across a wide spectrum of sea states. Interestingly, even at the transformation point of plunging breakers where higher-order theories were anticipated to perform better, linear theory provided accurate results.

Given that a single extreme wave can be responsible for the boulder displacement, we considered the maximum significant wave height statistically occurring during the weather event. Considering a Rayleigh distribution (Longuet-Higgins, 1952), the maximum wave height was computed as twice the significant wave height (Abadie et al., 2023). The corresponding maximum orbital velocity (V_{max}) was calculated under linear wave theory as:

$$V_{max}(z) = \frac{2\pi}{T_p}\frac{H_{max}}{2}\frac{cosh[k(h+z)]}{sinhkh} \tag{7}$$

where H_{max} is twice the significant wave height measured at the nearest point to the shore where the boulder is located during the passage of the hurricane, h is the water depth including tide and storm surge, T_p is the wave peak period, z is the vertical position within the water column and $k = 2\pi/\lambda$ is the wavenumber, with λ the wavelength, retrieved from depth and period according to the dispersion relation using a Newton-Raphson iterative method.

Applying linear wave theory (Eq. 7) for z = 0, the surface velocity is obtained as:

$$V_{max} = \frac{\pi H_{max}}{T_p}\frac{1}{tanh(kh)} \tag{8}$$

If we consider the wave orbital velocity at the seabed, linear wave theory (Eq. 7) for z = −h then writes:

$$V_{max} = \frac{\pi H_{max}}{T_p}\frac{1}{sinh(kh)} \tag{9}$$

4. Results

In the following, we present the analysis of five CBDs emplaced at four coastal sites alongshore Cuba by three different hurricanes. The sites are located on the South-Central coast (sites 1 and 2), the SE coasts (site 3) and the NE coast (site 4) of Cuba main Island (c.f. Fig. 1). More specifically, we detail the geomorphological analysis of each studied site and boulder, followed by results on the minimum flow velocity responsible for the boulder's emplacement using the equations of Nandasena et al. (2022) and the maximum wave orbital velocity produced by responsible hurricanes using linear wave theory.

4.1. Site 1: Punta Los Colorados Lighthouse

4.1.1. Geomorphological analysis

The site Punta Los Colorados Lighthouse is located ~2 km west of Hotel "Rancho Luna" and ~ 14 km south of Cienfuegos city (Figs. 1 and 5). The analysis concerns the two metric-scale boulders (Faro Colorado 1 and 2) on the low-lying coral reef terrace surface (T1) near the lighthouse (Fig. 5A, B, D, G).

The reef terrace T1 has a variable width along the coast, ranging from 10 to 150 m. The surface of the terrace where the CBD is emplaced, is free of sediment apron and consists of rugged reefal limestone with epikarst etched up to 1 m depth, probably enhanced by the periodic overwash from stormy weather and storm waves. The GPS profile of T1 shows elevations of 8.2 ± 1 m above sea level (m asl) at the lighthouse and 1.6 ± 0.5 m asl at the outer edge (Fig. 5E). The distal edge of the reefal terrace constitutes the modern shoreline and is characterized by a plunging sea cliff with small fractures and indentations generated by sea-directed runoff. About 1–2 m of the sea cliff is emerged, while ~ −2.5 m of the cliff is submerged. The fringing reef and associated reef crest are absent in this area. The offshore bathymetry is variable between −1.4 to −7.5 m as shown by the bathymetric profile surveyed 2 km eastwards (Fig. 5C). The sea floor in this area contains some coral colonies and sandy areas.

4.1.2. Faro Colorado boulders description

The boulders Faro Colorado 1 and 2 are accompanied by smaller boulders nearby. The two CBDs are located at ~69 m and ~ 117 m from the coastline at an elevation of ~5 m and ~ 7 m asl respectively (Fig. 5E, G). Faro Colorado 1 boulder is 3.90 m long, 2.65 m wide and 1.69 m high (Figs. 4A, B and 5B, E). The top of the boulder is rough, and the sides are slightly rounded. Its base is irregular, displaying a concave surface that has been exposed to abrasive wave action interpreted as a preserved tidal notch, suggesting that the boulder was pulled-off the shoreline from the sea cliff (Fig. 5B). Furthermore, we find corals colonies that are overturned with respect to their original growth position. The cliff adjacent to this boulder location is sufficiently high (~2 m) to produce a boulder of the observed size. Based on our interpretations, this boulder, detached from the cliff edge, was carried inland by rolling and deposited upside down (Fig. 5B). According to the lighthouse keeper, the boulder was emplaced during hurricane Lili in 2002 on the concrete foundation of what was an oxygen plant destroyed during this weather event (Fig. 5B).

The SfM point cloud of Faro Colorado 1 comprises ~184 million points, with an average point density of 435 pt./cm^2 (Table 1; Fig. 4B). We estimated the boulder volume to be 8.7 ± 1.6 m^3. Considering the measured boulder mean density of 2.40 g/cm^3, we obtained a boulder mass of 20.88 ± 3.8 tons (Table 2).

The Faro Colorado 2 CBD is 2.39 m long, 2.33 m wide and 1.39 m high (Fig. 5D, E). The surface of the northern side of the boulder is smooth while its southern side is rougher with erosion and dissolution

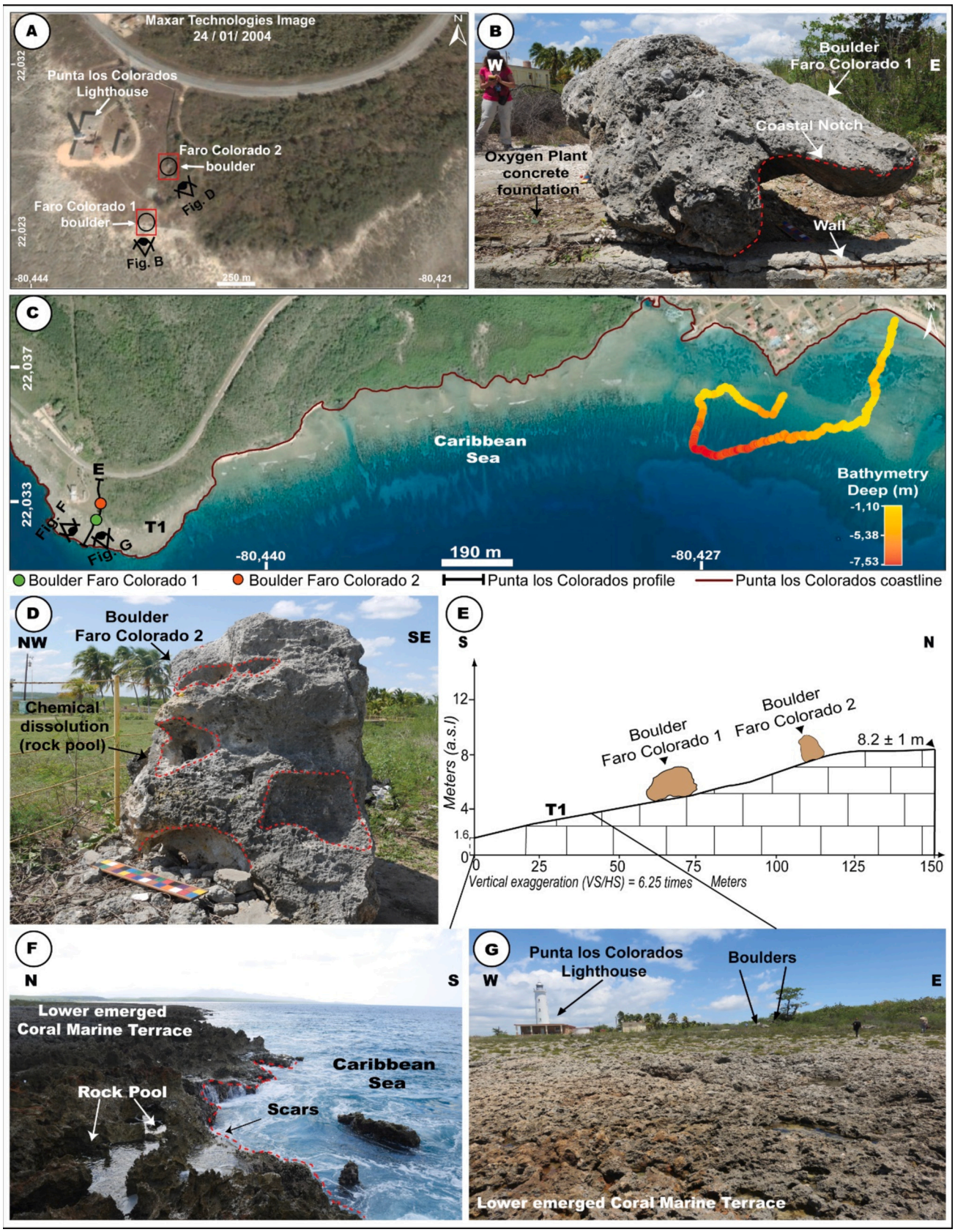

Fig. 5. Site Punta los Colorados Lighthouse and Faro Colorado 1 and 2 CBDs. (A) WorldView satellite imagery obtained in 2004 showing the coastal boulders in place. (B) and (D) Boulder morphology and dissolution marks. (C) Map of the bathymetric profile of Faro Colorado location, Cienfuegos. (E) Profile of the marine terrace of the site with the boulder emplacements (DGPS profile). (F) and (G) Interpreted field pictures of the coastal terrace.

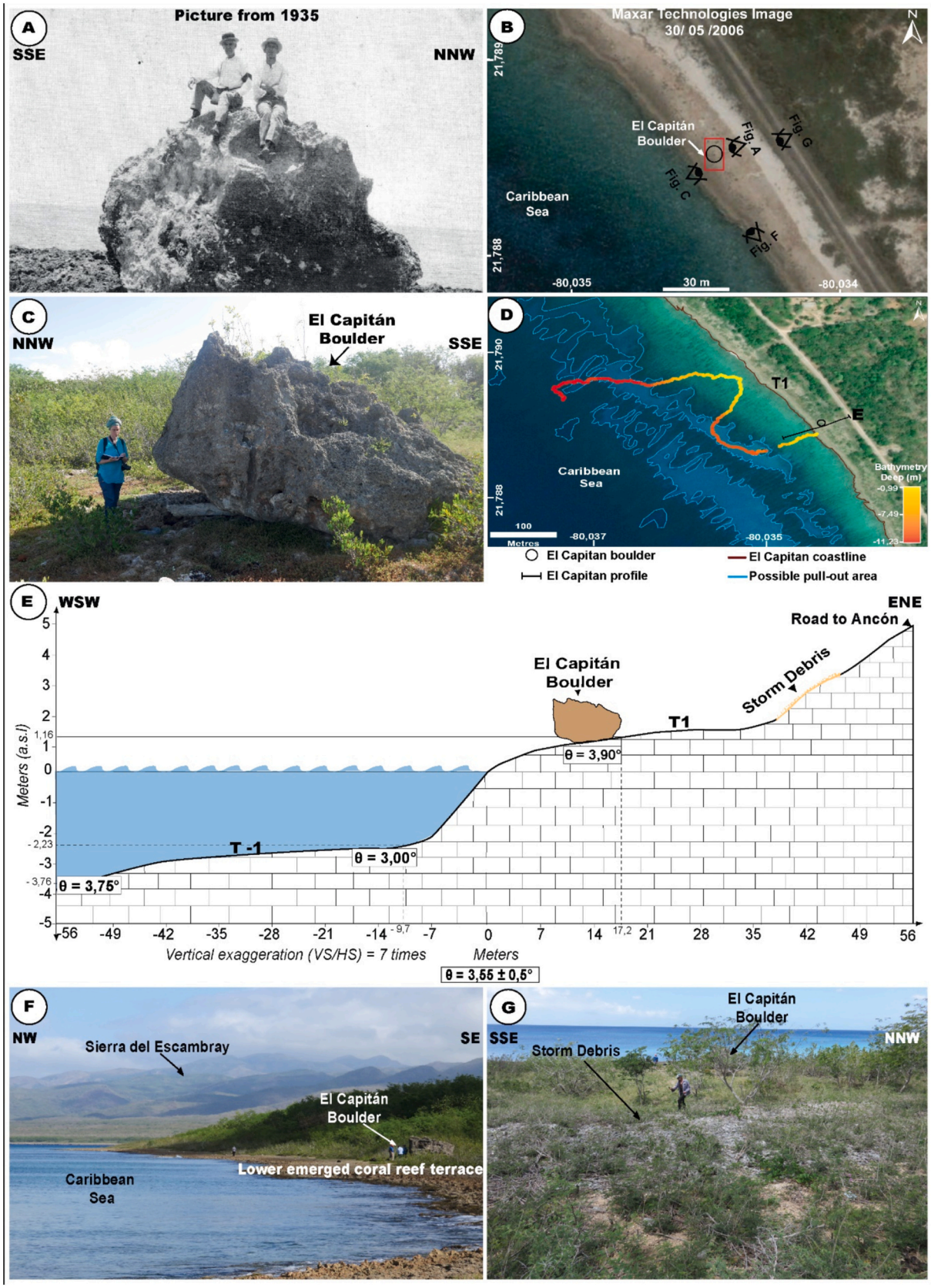

Fig. 6. Site Trinidad and the El Capitan coastal boulder. (A) Field picture after the passage of the 1935 Cuba Hurricane showing the El Capitan boulder, Source: Trinidad Municipal Historical Archive, Sancti Spíritus, Cuba. (B) WorldView satellite image obtained in 2006 showing the coastal boulder in place. (C) Morphology of the El Capitan boulder. (D) Map of the bathymetric profile location of Trinidad site. (E) Topographic and bathymetric profiles of the submerged platform (T-1) and emerged (T1) coral reef terrace with inclination angle and general view of Trinidad site (DGPS profile). (F) and (G) Interpreted field pictures.

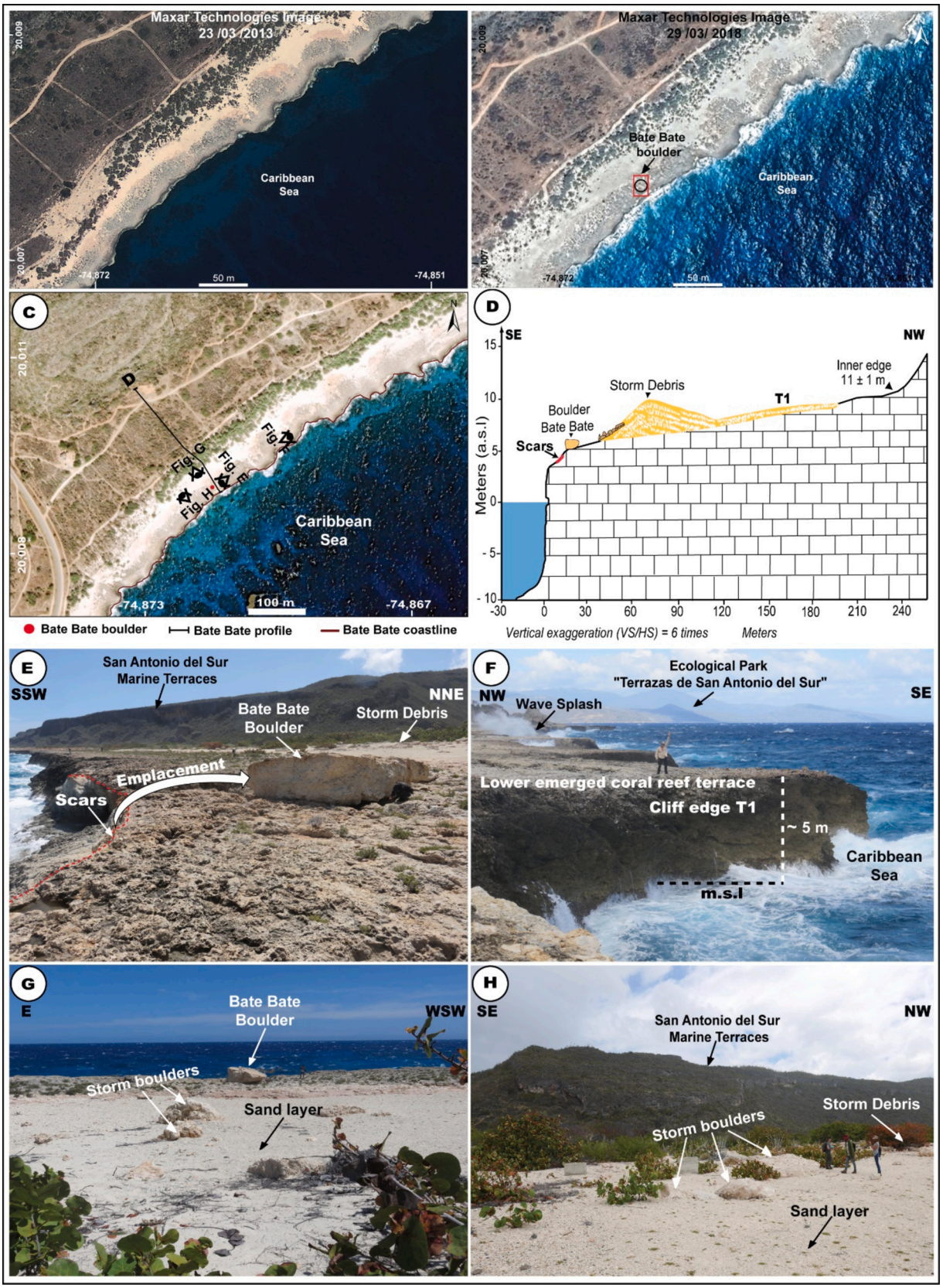

Fig. 7. Site Bate Bate and coastal boulder. (A) and (B) Temporal set of Worldview satellite imagery from 2013 to 2018 before and after the passage of the Hurricane Matthew. (C) Map of the topografic profile location in the Bate Bate Site. (D) Bathymetry and DGPS topographic profile of the coral reef terrace (T1). (E), (F), (G) and (H) Interpreted field pictures.

formed small rock pools with depth of ~25 cm similar to those observed on the surface of the coral reef terrace from which the boulders originate, akin to those seen on the surface of T1 (Fig. 5D, F). Furthermore, the seaward side of the boulder and its base are in contact with the storm debris and the a-axis of the boulder is slightly perpendicular to the base of the boulder (Fig. 5D). Based on these observations, we interpret that the boulder was detached from the outer edge of T1 and emplaced by overturning.

The SfM point cloud of Faro Colorado 2 includes ~18 millions, with an average point density of 185 pt./cm^2 (Table 1; Fig. 4C). We estimated a volume of 1.99 ± 0.3 m^3, and given the average density of Faro Colorado 2 (2.40 g/cm^3) provided a mass of 4.77 ± 0.7 tons (Table 2).

4.2. Site 2: Trinidad

4.2.1. Geomorphological analysis

The site "Trinidad" is located in the Trinidad municipality (Sancti Spíritus province), ~1.5 km south of "La Boca" beach and ~ 6 km SW of Trinidad city (Fig. 6). According to the specialists of the Center for Environmental Studies of Santi Spiritus city, El Capitan boulder is named by its proximity to the lodging "El Capitan" located to ~450 m from the boulder. The boulder was emplaced on a low-lying coral reef terrace (T1) at ~13 m from the shoreline.

The surface of the coastal terrace is rough, with numerous rocky pools (Fig. 8). The width of T1 is reduced and does not exceed 50 m. The coral reef terrace has an elevation of ~2 m at its inner edge and 1 m at its outer edge and exhibits slight seaward slope of 3.55 ± 0.5° (Fig. 6E). The marine terrace is covered by small fragments of storm debris, being well-developed ~25 m inland of the boulder location (Fig. 6E, G). In the Capitan area, the sea floor is shallow, ranging between −1 m and − 12.3 m in depth and it is gently sloping seaward. Landsat satellite images display high seafloor rugosity, interpreted as erosion areas and pull-out zones of the submerged platform (Fig. 6D).

4.2.2. El Capitan boulder description

According to the municipal archives of Trinidad municipality, El Capitan boulder was emplaced on the coastal terrace during the 1935 Cuba Hurricane (Fig. 6A). The morphology of the boulder is elongated, being 6.10 m long, 3.90 m width and 2.85 m in height (Fig. 6A, C, E). The base of the boulder is partly flat and irregular. The top of the boulder is rough, as well as its sides. Some corals colonies identified on the sides of the boulder are in normal growth position showing that the boulder is not overturned. Based on these observations, and because of the absence of a cliff on the edge of the coastal terrace, we propose that El Capitan boulder was detached from the submerged adjacent platform, which is the case for the majority of boulders in the Trinidad region (León-Brito et al., 2021).

The SfM point cloud comprises ~133 million points with an average point density of 347 pt./cm^2 (Table 1; Fig. 4E). Shown in Table 2, we estimated a volume of 29.2 ± 3.1 m^3 and a mass of 74.75 ± 7.9 tons (average density of 2.56 g/cm^3).

4.3. Site 3: Bate Bate

4.3.1. Geomorphological analysis

The site "Bate Bate" is located in the municipality of "San Antonio del Sur", ~3 km south of the town "Baitiquirí" and ~ 40 km NW of Guantanamo province (Fig. 7). The boulder is located at ~10 m from the coastline on the low-lying coral reef terrace (T1).

There, the coral reef terrace T1 is ~230 m wide, it has an elevation of ~11 m at its inner edge and 5 to 6 m at its outher edge (Fig. 7D, F). We found a well-developed *Camellon de Tormenta* at ~30 m from the cliff edge with numerous boulders essentially <1 m in length, organized in a sandy matrix including bioclasts (corals, bivalves, gastropods), together with larger boulders on the nearshore side resulting from extreme storm/hurricane wave events (Fig. 7G, H). The outer edge of T1 is irregular and characterized by indentations that we interpret as generated by sea-directed runoff, in addition to rocky pools on the marine terrace. Between 8 and 10 m of coastal cliff is submerged and 5 to 6 m of the cliff are emerged (plunging cliff, type-C platform, Sunamura, 1992; Fig. 7D). Bathymetric data show depths from −17 to −78 m, with slopes between 17° and 21° up to about −500 m, whereas up to −1500 m the slope is ranging from 12° and 17° (Álvarez Ortiz et al., 2019). The steep slopes are most probably the cause of the absence of modern coral reefs in this area.

4.3.2. The Bate Bate boulder description

The so-called Bate Bate boulder is one of the largest boulders on the distal part of T1 found at this site (Fig. 7G, H). It is located at ~9 m from the convex cliff edge. The sea cliff displays a fresh scar that Beltrán-Fonseca (2019) argues as the mark of the boulder original position (Fig. 7E).

The boulder morphology is elongated with length of 7.46, width of 3.85 m and height of 1.95 m (Fig. 7E). The base of the boulder is irregular, the top surface is relatively flat. The sides of the boulder are also irregular and subvertical. The boulder is upside down, as evidenced by the coral colonies found in inverted growth position. Likewise, the upper surface of the boulder shows less weathering than the terrace substrate on which it is located. According to these observations, and in agreement with the interpretation of Beltrán-Fonseca (2019), we propose that the boulder was emplaced by rolling and overturning after detachment from the active sea cliff.

The SfM point cloud of this boulder comprehends ~86 million points, with an average point density of 209 pt./cm^2 (Table 1; Fig. 4D). The volume was found to be 25.9 ± 2.6 m^3, and considering a density of 2.59 g/cm^3, we estimated a mass of 67.08 ± 6.7 tons (Table 2).

4.4. Site 4: Bahia de Boma

4.4.1. Geomorphological analysis

The "Bahia de Boma" site is located on the NE shore of Cuba Island, in the municipality of "Baracoa" at ~6 km W of the town of "Baracoa", and at ~6 km E from "Mata Bay" in Guantánamo province (Fig. 8). The boulder is located on the lower coastal terrace (T1).

The coastal terrace T1 is highly eroded and includes numerous rock pools. The boulder under investigation is located at an elevation of ~6 m asl and the distal edge of T1 is located at ~5 m asl. On T1, we found several large boulders, all emplaced by extreme waves. Four of these boulders were emplaced by Hurricane Matthew as indicated by witnesses/satellite images scouting (Fig. 8B, C, F). The distal edge of T1 is characterized by small indentations generated by sea-directed runoff with rock pools. Vertical sea cliffs show scars, suggesting the original location of the detached boulders. The depth in front of the cliff edge is −5.4 m asl (plunging cliff, type-C platform, Sunamura, 1992; Fig. 8E). The development of modern coral reefs is not observed in the study area, perhaps due to the steep slopes (between 10° and 13°) combined with the deep bathymetry (Álvarez Ortiz et al., 2019).

4.4.2. The Bahia de Boma boulder description

The Bahia de Boma boulder is located ~38 m from the modern sea cliff which exhibits a "fresh" area that we identify as the detachment zone of this boulder (Fig. 8B, I). Furthermore, on Worldview satellite images, we were able to identify the trace of the trajectory of the boulder after detachment. This occurred during Hurricane Matthew in 2016 as seen on the satellite images (Fig. 8A, B, I) and this information was corroborated with specialists from the Center for Environmental Studies of the National Park "Alejandro de Humboldt" in Baracoa region. The Bahia de Boma boulder is elongated and relatively flat, being 9.7 m long, 4.4 m wide and 2.4 m high (Fig. 8H). The base of the boulder is irregular. The sides of the boulder are rough and subvertical. The upper surface of the boulder displays minimal weathering effects in comparison with the T1 surface and the dissolution pools at the base of the boulder, similar to

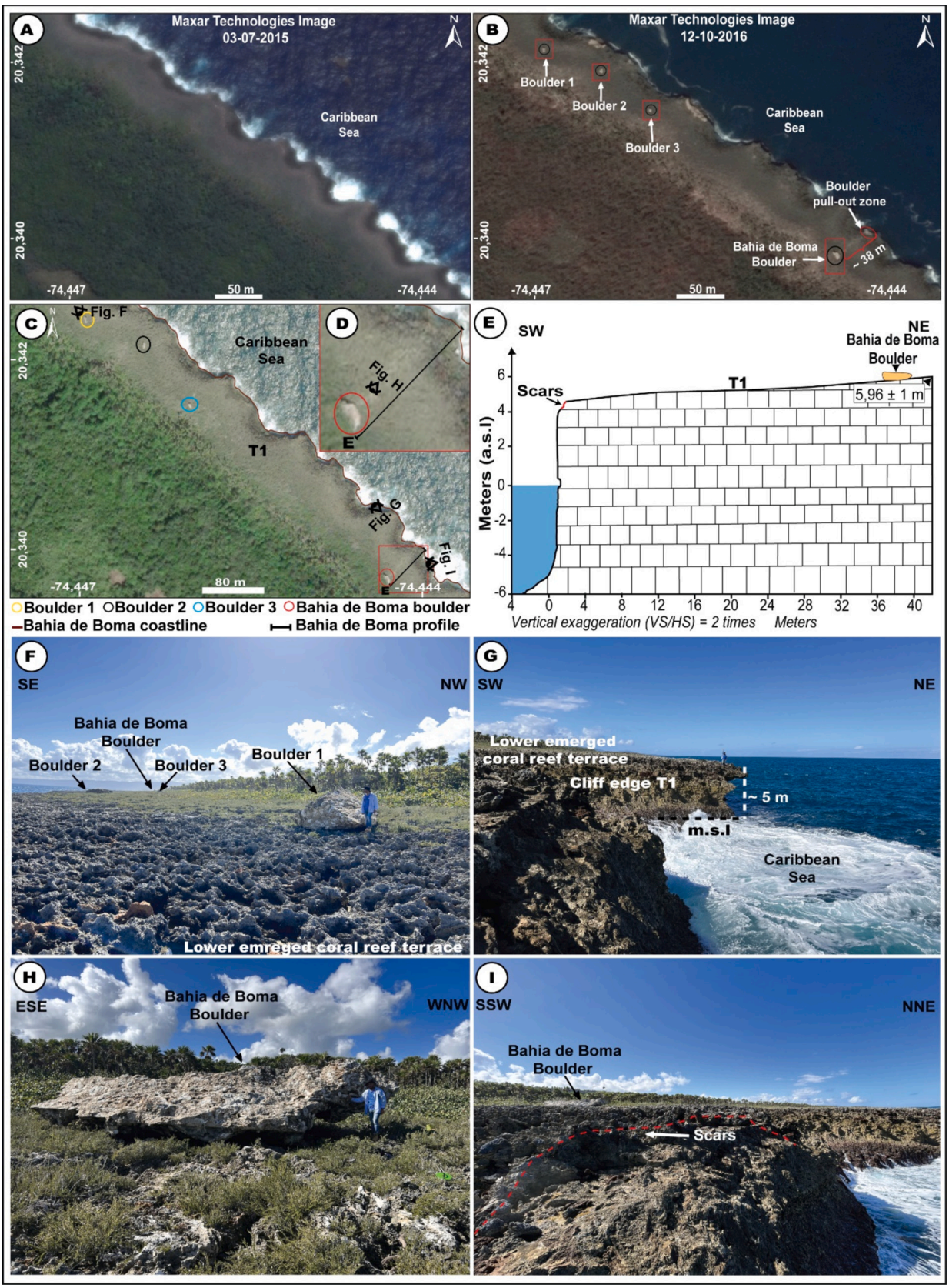

Fig. 8. Site Bahia de Boma and coastal boulder. (A) and (B) Worldview satellite imagery from 2015 to 2016 before and after the passage of the Hurricane Matthew. (C) Map of the topographic profile location in the site Bahia de Boma. (D) (inset) Topographic profile in the site Bahia de Boma. (E) Bathymetry and general view of Bahia de Boma boulder (DGPS profile). (F), (G), (H) and (I) Interpreted field pictures.

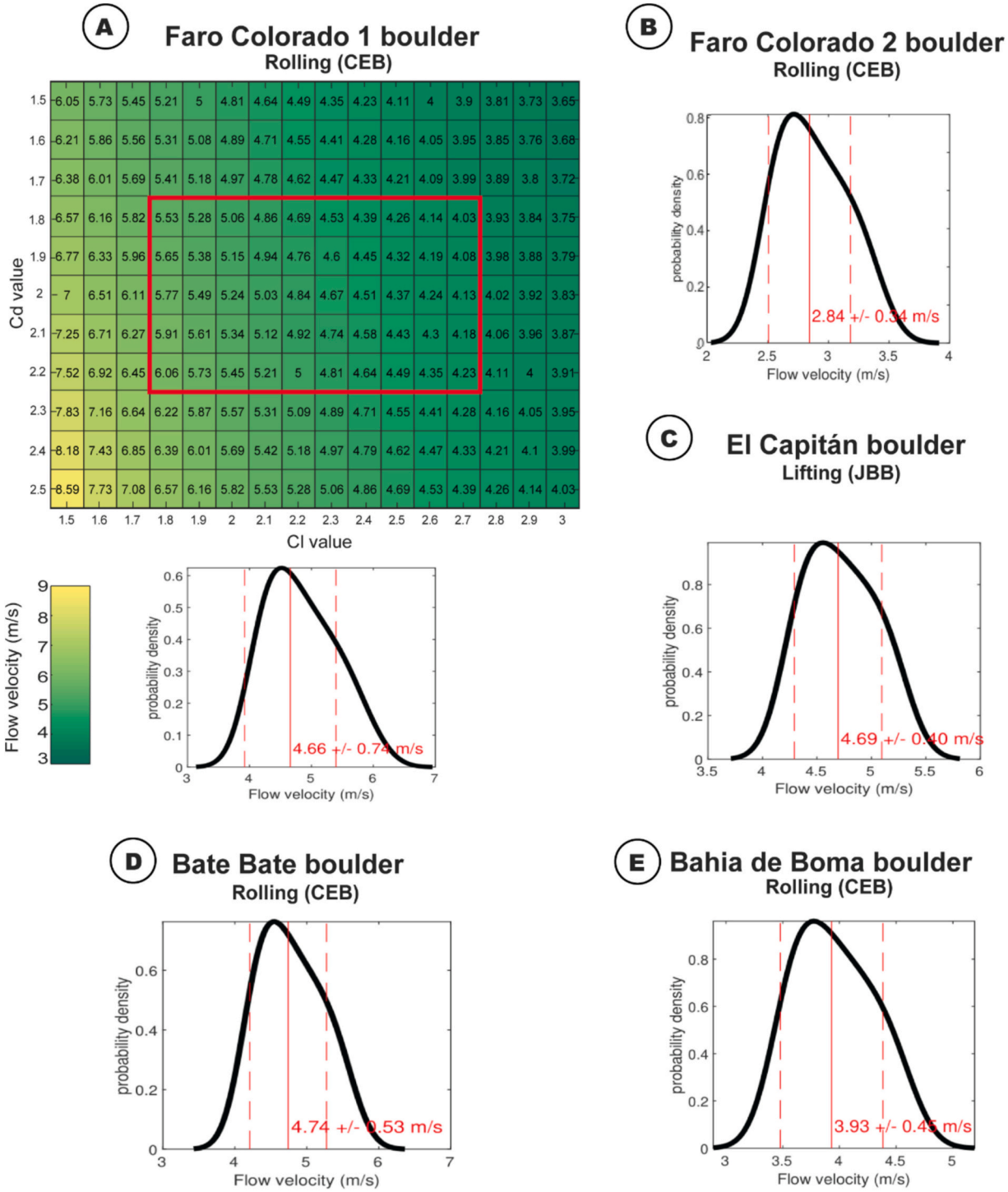

Fig. 9. Solving through Nandasena et al. (2022) equations for minimum flow velocity *(u)* required to transport the boulders using ranges of Cl values between 1.8 and 2.7 and Cd values between 1.8 and 2.2. (A) Minimum flow velocity for the Faro Colorado 1 boulder. The lower inset shows the distribution of minimum flow velocity and the 1-sigma standard deviation for: (A) Faro Colorado 1 boulder, (B) Faro Colorado 2 boulder, (C) El Capitan boulder, (D) Bate Bate boulder and (E) Bahia de Boma boulder.

those observed at the surface of T1. Within the limestone forming the boulder, coral colonies are in inverted growth position, indicating that the boulder is resting upside down. Based on all these geomorphologic evidences, we hypothesize that the boulder was detached by the hurricane Matthew and deposited overturned (Fig. 8H).

As shown in Table 1 and Fig. 4F, the SfM point cloud is composed of ~180 million points with an average point density of 397 pt./cm^2. We estimated a volume of 31.5 ± 2.5 m^3. Considering an average density of 2.37 g/cm^3, we calculated a mass of 74.65 ± 5.9 tons (Table 2).

4.5. *Minimum flow velocity responsible for the emplacement of boulders*

In this section, we present the results of the application of the hydrodynamic equations of Nandasena et al. (2022) to the five coastal boulders. We hypothesized (see section 4.1) that the Faro Colorado 1 and 2 boulders originated from the cliff-edge and were emplaced by

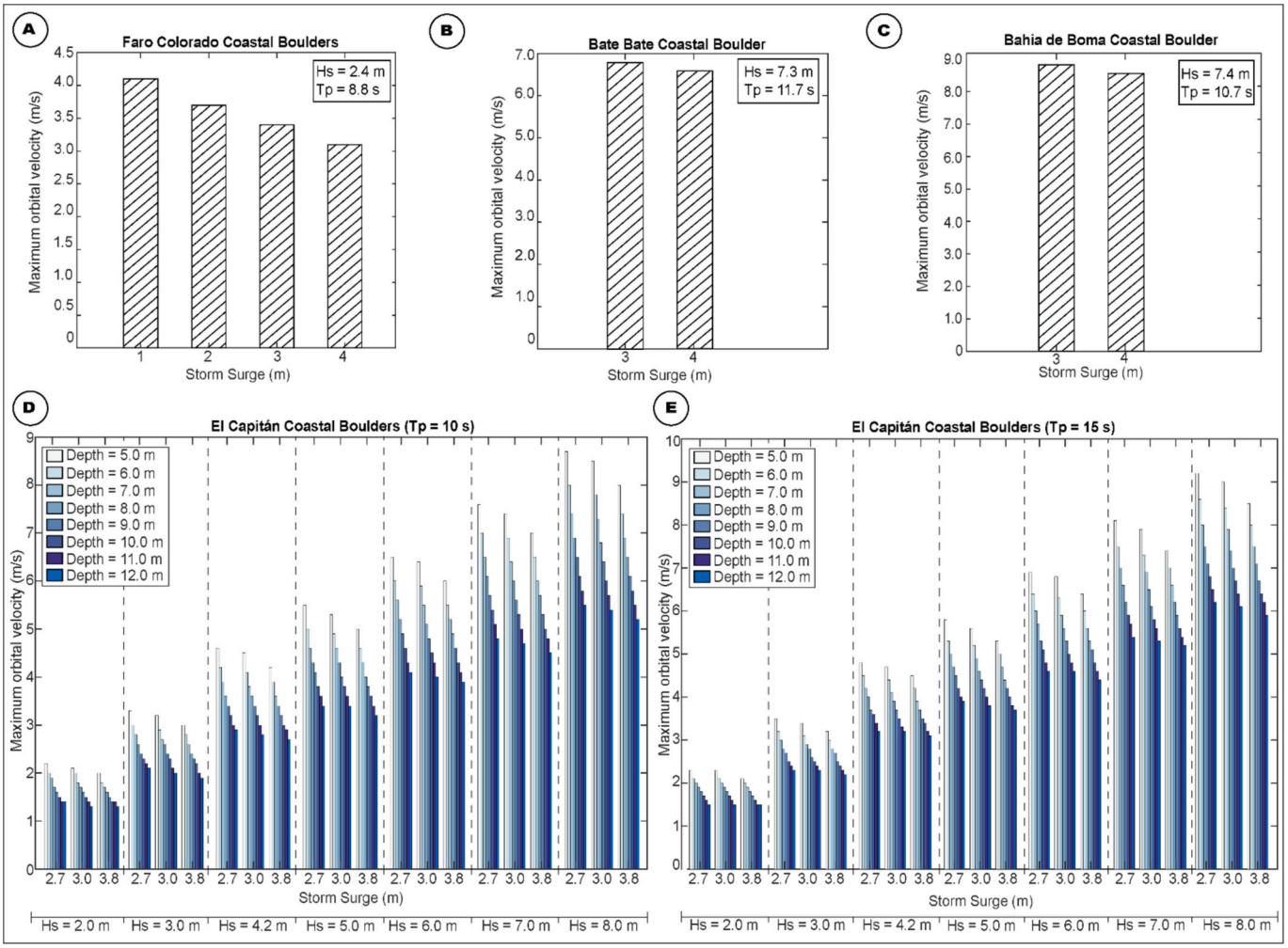

Fig. 10. Maximum orbital velocity for the three hurricanes responsible for the emplacement of the five studied boulders, considering different hypotheses of storm surge, wave height and water depth. (A) Hurricane Lili in 2002 in the Trinidad region. (B) Hurricane Matthew in 2016 in the Bate Bate region. (C) Hurricane Matthew in 2016 in the Baracoa region. (D) and (E) 1935 Cuba Hurricane in the Trinidad region.

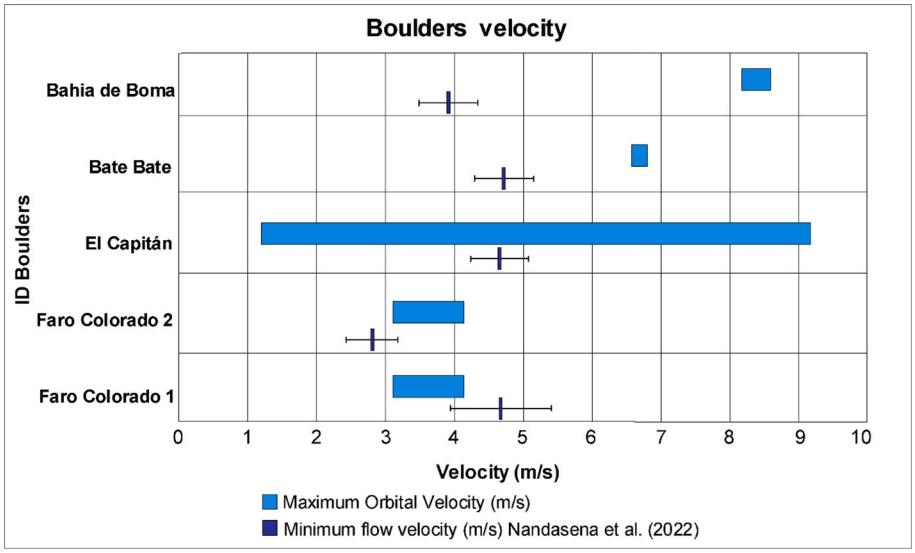

Fig. 11. Calculated values of minimum flow velocity for the studied boulders and the values of maximum orbital velocity for the hurricanes responsible for their emplacement.

overturning (Fig. 5; Table 2). Under this assumption, the minimum flow velocity required to emplace the Faro Colorado 1 boulder was calculated to be 4.66 ± 0.74 m/s (mean ± 1 std.; Fig. 9A) and for the Faro Colorado 2 boulder of 2.84 ± 0.34 m/s (Fig. 9B). For the El Capitan boulder, we suggested (see section 4.2) that the boulder was a joint-bounded boulder originating from the submerged platform emplaced by saltation/lifting (Fig. 5; Table 2). Under these conditions, the minimum flow velocity required to emplace the boulder is 4.69 ± 0.40 m/s (Fig. 9C). We calculated the minimum flow velocity required to emplace the Bate Bate boulder to be 4.74 ± 0.53 m/s (Fig. 9D), considering that the boulder came from the cliff-edge and the type of emplacement was overturning (see section 4.3). Finally, for the Bahia de Boma boulder, transported from the cliff edge and overturned (section 4.4), we calculated the minimum flow velocity required for its emplacement to be 3.93 ± 0.45 m/s (Fig. 9E).

4.6. Maximum orbital velocity

Using linear wave theory, and considering the water depth at the initial boulder location, we calculated the maximum wave orbital velocity for the different hurricanes responsible for the emplacement of the studied boulders (Fig. 10).

We estimated a maximum orbital velocity during the passage of Hurricane Lili in 2002 in Cienfuegos coastline to be between 3.1 m/s and 4.1 m/s. This estimation was based on hydrodynamic parameters (storm surge, wave height and wave period) for this hurricane provided by WAVEWATCH III® Production Hindcast and a water depth at the sea-cliff of −2.5 m (Fig. 10A). Using this approach, the maximum orbital velocity produced by hurricane Matthew in 2016 when fronting the Bate Bate coastline ranged between 6.6 m/s and 6.8 m/s (Fig. 10B) and for the Bahia de Boma coastline the values ranged between 8.2 m/s and 8.6 m/s (Fig. 10C).

For the 1935 Cuba Hurricane we estimated the maximum orbital velocity considering the range of hydrodynamical values for category 3 hurricanes proposed by NOAA Ocean Explorer (2013) along with a range of bathymetric values of the offshore platform where areas of stripping have been observed (−5 m to −12 m) because we do not know the exact origin of the Capitan boulder (Fig. 6D). Due to large uncertainties for this boulder, we consequently obtained a wide range of values for the maximum orbital velocity, from 1.3 m/s to 9.2 m/s (Figs. 10D, E and 11).

5. Discussion

The overall aim of this study was to advance the understanding of coastal boulder emplacement under the influence of waves by using theoretical and empirical tools to evaluate hydrodynamic conditions. For that, we took advantage of the important record of CBDs along Cuba shoreline. In the following sections, we first discuss the maximum wave orbital velocity during the considered hurricanes, obtained from linear wave theory, and compare it with the minimum flow velocity values derived from the hydrodynamic equations of Nandasena et al. (2022) which make use of boulder geometry and field setting. Then, we analyze the minimum flow velocity results deduced from the boulders' morphology in relation to similar studies at other locations worldwide.

5.1. Comparison of the maximum wave orbital velocity with the minimum flow velocity deduced from boulder analysis

In most cases, our results show that the minimum flow velocity calculated (minimum estimate) from hydrodynamic equations and boulder characteristics is lower than the maximum wave orbital velocity during the weather event, therefore indicating that the Nandasena et al. (2022) equations provide appropriate results for boulder emplacement analysis for our studied cases (Fig. 11).

In Bate Bate, maximum wave orbital velocities of between 6.6 and 6.8 m/s during Hurricane Matthew in 2016 (Figs. 10B and 11) agree well with the minimum flow velocity values calculated using Nandasena et al. (2022) equations, with values of 4.39 ± 0.57 m/s. For the same hurricane, in the Bahia de Boma region, we obtained maximum orbital velocities ranging between 8.2 m/s and 8.6 m/s (Figs. 10C and 11), which again surpass the minimum flow velocity calculated for the Bahia de Boma (3.93 ± 0.45 m/s). Likewise, the minimum flow velocity deduced from the Faro Colorado 2 boulder (2.84 ± 0.34 m/s) is below the maximum orbital velocity produced by Hurricane Lili 2002 in the study area, which according to our results ranges between 3.1 and 4.1 m/s (Figs. 10A and 11).

For the Faro Colorado 1 boulder, the range of plausible minimum flow velocity values (4.66 ± 0.74 m/s) are higher than the maximum orbital velocity, which ranges from 3.1 m/s and 4.1 m/s (Figs. 10A and 11). However, the minimum flow velocity should be lower than or equal to the maximum orbital velocity during the weather event in order to validate hydrodynamics equations relating boulder characteristics to flow conditions at the time of emplacement. This mismatch may be explained by the fact that the wave parameters provided by NOAA Environmental Modeling Center (2023) correspond to average values, possibly from a distal part of the coast. In this regard, local wave amplification could have occurred for this site, in particular due to the shallow depth of the submerged platform associated with the low cliff height, which could not be quantified using linear wave theory. Linear wave theory tends to simplify or ignore the interaction of waves with seafloor topography, which can significantly influence wave behavior. Additionally, the presence of a cape at the Faro Colorado site can significantly influence the alongshore distribution of wave energy at the coast, and as a result, it is possible that larger waves be occurring in reality than those theoretically calculated from far-field data (Fig. 5).

Concerning the 1935 Cuba Hurricane, we obtained a very large range of maximum orbital velocities, from 1.3 m/s to 9.2 m/s (Fig. 10D and E). The minimum flow velocity values calculated from the hydrodynamic equations of Nandasena et al. (2022), 4.69 ± 0.40 m/s, is higher than most of the maximum orbital velocity values (59.3 % of values; Fig. 11). However, if we consider the highest values of maximum orbital velocity, these are higher than the calculated minimum flow velocity values. These results indicate that under these conditions, both minimum flow and maximum orbital velocities are consistent. These consistent values of maximum orbital velocity require a wave height, storm surge and period equivalent to those occurring during hurricanes that affected Cuba with comparable intensity to the 1935 Cuba Hurricane. For example, during Hurricane Michelle that made landfall at Playa Giron between 4 and 5 November 2001, with a category 3 and a storm surge of 3 m at Cayo Largo, Cuba (Fig. 1; Beven, 2002). This hurricane produced a significant wave height of 7.7 m with a peak period of 10.3 s in the vicinity of the Bahía de Cochinos (Playa Giron, Cuba, Fig. 1; NOAA Environmental Modeling Center, 2023). Also, during Hurricane Charley that entered the province of Artemisa on August 13, 2004, with a category 3 and a storm surge of 3.9 m at Playa Cajío, Cuba (Pasch et al., 2011; Fig. 1), NOAA Environmental Modeling Center (2023) shows a significant wave height of 7.9 m with a period of 13.3 s.

Despite the limitations of linear wave theory, we believe it is a valuable tool in studies of this type due to its simplicity and ease of application, and since the input (wave parameters) are increasingly available. In our research, we focused on five CBDs emplaced by three recent hurricanes, and a key achievement was to reconcile theoretical approaches that utilize the morphology of the boulders and their geomorphic context with the hydrodynamic conditions that caused their emplacement. Future studies should encourage integrating a more precise description of wave transformation, for instance by considering non-linear aspects and more complex considerations such as those incorporated in hydro-sedimentary models such as XBeach.

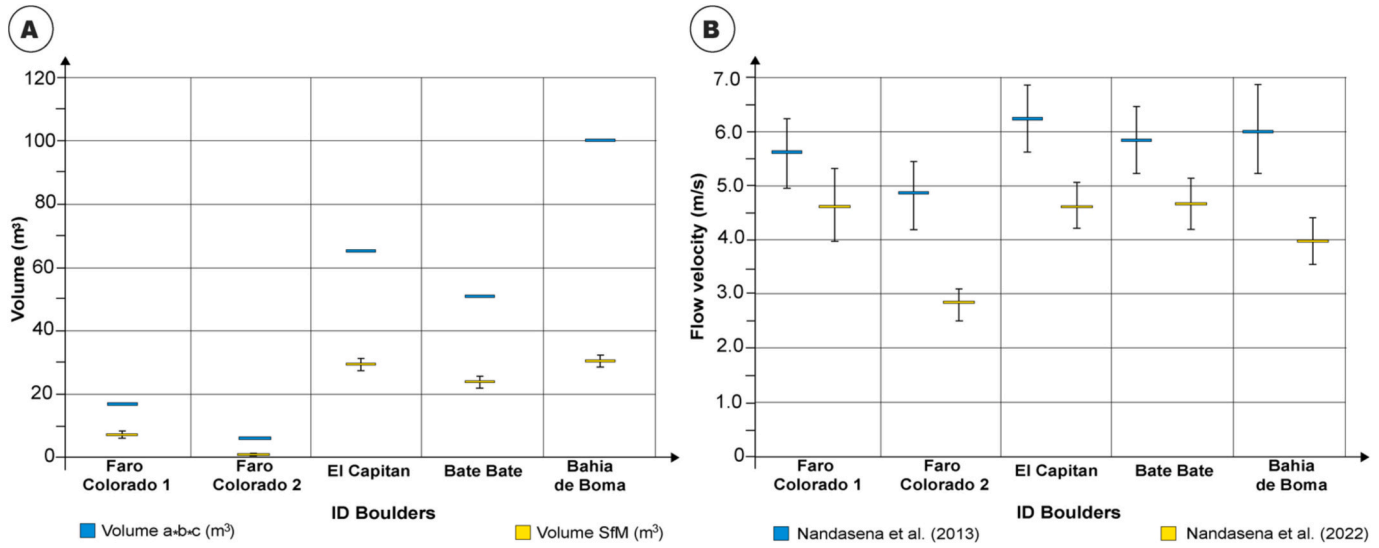

Fig. 12. Comparison between: A) the volume obtained from the method of the three boulder axes and the volume obtained using SfM photogrammetry; B) the corresponding minimum flow velocities (mean ± 1 std.) calculated using Nandasena et al. (2013) and Nandasena et al. (2022) equations, respectively.

5.2. Flow velocity values deduced from the storm boulders morphology at other locations

Minimum flow velocities responsible for boulder emplacement obtained in this study, ranging from 2.84 ± 0.34 m/s to 4.74 ± 0.53 m/s, are similar to those modelled by Goto et al. (2009). In their study, the authors derived minimum flow velocity values of 3.1–6.5 m/s for boulders on the reef flat of Kudaka Island, Japan, emplaced by Typhoon (200704) (MAN-YI) in 2007 (Category 4 - equivalent super Typhoon).

However, the values of our study are lower than those modelled in the Bahamas for a storm of lower energy ("Perfect Storm" in 1991), whereby a mean flow velocity of 6.0 m/s was computed (Rovere et al., 2017). They are also lower than those obtained for Hurricane Sandy in 2012 (category 2), with a computed flow velocity of 10.2 m/s (Rovere et al., 2017). However, Hearty and Tormey (2018) raised doubts about these findings, and argued that the minimum flow velocity values were probably exaggerated. Indeed, calculations in Rovere et al. (2017) do not take into account the local and regional geology and stratigraphic provenance of the boulders. Another limitation being the method used to calculate the volume of the boulders, which was approximate, since the 3D boulder geometry was simplified to cuboidal (Nandasena et al., 2013), although a photogrammetric procedure was applied.

Based on our results, we show that the determination and use of boulder volume derived precisely with SfM photogrammetry will contribute to reduce minimum flow velocity values (Table 2; Fig. 12), although a common limitation is that it cannot reconstruct part of the boulder base, resulting in it being considered as flat. In the absence of a precise 3D model of coastal boulders, recent work (e.g., Khalfaoui et al., 2024) continued to have recourse to initial hydrodynamic equations whereby boulder volume is approximated to cuboidal shape. Pedoja et al. (2023) made a comparison between the flow velocity calculated by Nandasena et al. (2013) (equation with the three axes volume calculation approach) and the equation of Nandasena et al. (2022) (equation with the SfM volume calculation approach), for a 210 tons boulder in Cuba. They observed an overestimation of the minimum flow velocity computed using equations in Nandasena et al. (2013). Extending this comparison to the five boulders studied herewith (Fig. 12B), we corroborate this finding. Equations that assume a cuboidal shape systematically overestimate the minimum flow velocity values for all the boulders studied. The equations of Nandasena et al. (2022) also resulted in reduced variability around the mean flow velocity computed, which is attributable to the improved volume and mass calculations, through the inclusion of the projected areas of the boulders in the calculations.

6. Conclusions

This study analyzed five coastal boulder deposits emplaced by three recent hurricanes on low marine terraces alongshore Cuba Island. We estimated their volume ranging from 1.99 ± 0.3 to 31.5 ± 2.5 m^3, density from 2.40 to 2.59 g/cm^3 and mass from 4.77 ± 0.7 to 74.75 ± 7.9 tons. Based on geomorphological observations, we elucidated their mode of emplacement. Using this data, we calculated the minimum flow velocity needed for their emplacement, with results ranging from 2.84 ± 0.34 to 4.74 ± 0.53 m/s. These values were compared with the maximum orbital velocity estimated for the hurricanes responsible for the boulders' emplacement, with values ranging from 1.3 to 9.2 m/s. The comparison between velocities showed that for all sites except one, there is a good agreement between minimum flow velocities and maximum orbital velocities, with minimum flow velocities for boulder emplacement consistently smaller than the maximum wave orbital velocity during the weather event. The difference observed for one boulder is attributed to specific site effects, highlighting in this case the limitation of using distant hydrometeorological data for characterizing wave processes responsible for coastal boulder deposits. For the only site where the order is reversed, the reason was attributed to potential site effects that could locally increase the maximum wave height and thus maximum orbital velocity. This new study opens the door for a better determination of the magnitude and typology of past extreme wave events using recent hydrodynamical equations, while emphasizing the importance of correctly considering the morphology of the entire coastline, in order to improve our understanding of coastal hazards.

Software

CloudCompare *V*2 (version 2.7.0) [GPL software]. Retrieved from http://www.cloudcompare.org

MeshLab (version 2023.12) [GPL software]. Retrieved from https://www.meshlab.net/

Agisoft Metashape Professional (version 1.7.2 build 12070). Retrieved from https://www.agisoft.com/

The ESRI's ArcGIS (version 10.8.1). Retrieved from https://www.esri.com [Software].

CRediT authorship contribution statement

Pedro Dunán-Avila: Writing – review & editing, Writing – original draft, Visualization, Validation, Software, Methodology, Investigation, Formal analysis, Data curation, Conceptualization. **Christine Authemayou:** Writing – review & editing, Validation, Supervision, Project administration, Methodology, Investigation, Formal analysis, Conceptualization. **Marion Jaud:** Writing – review & editing, Software, Methodology, Investigation, Formal analysis, Conceptualization. **Kevin Pedoja:** Writing – review & editing, Validation, Methodology, Investigation, Formal analysis, Conceptualization. **Julius Jara-Muñoz:** Writing – review & editing, Validation, Software, Methodology, Formal analysis. **Stephane Bertin:** Writing – review & editing, Validation, Software, Methodology, Investigation, Formal analysis. **Leandro Peñalver-Hernández:** Writing – review & editing, Validation, Project administration, Methodology, Investigation, Conceptualization. **France Floc'h:** Writing – review & editing, Validation, Software, Methodology, Investigation, Formal analysis. **Arelis Nuñez-Labañino:** Writing – review & editing, Validation, Methodology, Investigation. **Patricio Winckler:** Writing – review & editing, Software, Investigation. **Jean Pierre-Toledo:** Writing – review & editing, Software, Investigation. **Pedro Benítez-Frometa:** Writing – review & editing, Methodology, Investigation. **Hassan Ross-Cabrera:** Writing – review & editing, Methodology, Investigation. **Pauline Letortu:** Writing – review & editing, Software. **Angel Raúl Rodríguez-Valdés:** Writing – review & editing, Investigation. **Noel Coutín-Lobaina:** Writing – review & editing, Investigation. **Denovan Chauveau:** Writing – review & editing, Validation, Investigation.

Declaration of competing interest

The authors declare that they have no known competing financial interests or personal relationships that could have appeared to influence the work reported in this paper.

Acknowledgements

This work was supported by public funds received in the framework of a project (ANR-10-EQPX-20) of the program "Investissements d'Avenir" managed by the French National Research Agency. It was also supported by the ISblue projects, Interdisciplinary graduate school for the blue planet (ANR-17-EURE-0015, E*V*EBloCo), a national INSU TelluS project (TECIBO), the PHC Carlos (PROJET N°49740YL, Campus France) scientific cooperation program. We sincerely thank the French Embassy in Cuba for their invaluable support in facilitating our mobility. We would like to sincerely thank the two anonymous reviewers and editor for their thoughtful insights and valuable feedback. Their contributions have greatly helped to improve the quality and clarity of our work.

Appendix A. Supplementary data

Supplementary data to this article can be found online at https://doi.org/10.1016/j.margeo.2024.107438.

Data availability

Boulder 3D models can be found at doi: https://doi.org/10.5281/zenodo.12633934 and the additional data is accessible in supplemental materials.

References

Abadie, S., Burkhart, E.P., Parvin, A., 2023. Large concrete block displaced by a rogue wave: analysis of an event incidentally captured by a photographer. In: EGU General Assembly 2023, Vienna, Austria, 24–28 Apr 2023, EGU23-3336. https://doi.org/10.5194/egusphere-egu23-3336.

Aguirre Feria, G.M., Matos Pupo, F., Sánchez Loyola, A., 2021. Estudio bibliométrico sobre la producción científica de huracanolitos en la costa de Cuba. Avances 23 (1), 40–60.

Álvarez Ortiz, M., Leyva Ramos, E., Salazar Pérez, C.F., Benítez Tabares, J.G., LLuveras Pérez, G., Prieto Querol, M.E., 2019. Informe Científico -Técnico, "Cartografía del Borde Superior del Talud Insular de Cuba"..

Araoka, D., Yokoyama, Y., Suzuki, A., Goto, K., Miyagi, K., Miyazawa, K., Matsuzaki, H., Kawahata, H., 2013. Tsunami recurrence revealed by Porites coral boulders in the southern Ryukyu Islands, Japan. Geology 41 (8), 919–922.

Authemayou, C., Nuñez, A., Pedoja, K., Peñalver, L., Chauveau, D., Dunán-Avila, P., Martin-Izquierdo, D., de Gelder, G., Husson, L., Castellanos Abella, E., de Benítez Frómeta, P.J., Pastier, A., 2023. Oblique Collision of the Bahamas Platform at the Northern Boundary of the Caribbean Plate Recorded by the late Cenozoic Coastal Terraces of SE Cuba. Tectonics 42 (8). https://doi.org/10.1029/2023TC007806.

Barbano, M.S., Pirrotta, C., Gerardi, F., 2010. Large boulders along the south-eastern Ionian coast of Sicily: storm or tsunami deposits? Mar. Geol. 275 (1–4), 140–154. https://doi.org/10.1016/j.margeo.2010.05.005.

Beltrán-Fonseca, B., 2019. Huracanolitos en Baitiquirí (Guantánamo), movidos por el huracán Matthew: análisis del proceso físico. Aplicación en estudios de paleodeposiciones. Universidad Central "Marta Abreu" de Las Villas.

Benner, R., Browne, T., Brückner, H., Kelletat, D., Scheffers, A., 2010. Boulder Transport by Waves: Progress in Physical Modelling. Zeitschrift Für Geomorphol. Supplemen. Issu. 54 (3), 127–146. https://doi.org/10.1127/0372-8854/2010/0054S3-0022.

Beven, J., 2002. Tropical Cyclone Report Hurricane Michelle 29 October - 5 November 2001. https://www.nhc.noaa.gov/data/tcr/AL152001_Michelle.pdf.

Boesl, F., Engel, M., Eco, R.C., Galang, J.B., Gonzalo, L.A., Llanes, F., Quix, E., Brückner, H., 2020. Digital mapping of coastal boulders – high-resolution data acquisition to infer past and recent transport dynamics. Sedimentology 67 (3), 1393–1410. https://doi.org/10.1111/sed.12578.

Boulton, S.J., Whitworth, M.R.Z., 2018. Block and boulder accumulations on the southern coast of Crete (Greece): evidence for the 365 CE tsunami in the Eastern Mediterranean. Geol. Soc. Lond. Spec. Publ. 456 (1), 105–125. https://doi.org/10.1144/SP456.4.

Bourgeois, J., Mac Innes, B., 2010. Tsunami Boulder Transport and Other Dramatic Effects of the 15 November 2006 Central Kuril Islands Tsunami on the Island of Matua. Zeitschrift Für Geomorphologie, Supplementary Issues, pp. 175–195.

Bourman, R.P., Panda, D., Buckman, S., Banerjee, D., Ryan, D., White, L.T., 2023. Tsunami or storm ? A high-level coastal boulder field on the southern tip of Eyre Peninsula, South Australia ARTICLE HISTORY. Aust. J. Earth Sci. 0 (0), 1–15. https://doi.org/10.1080/08120099.2023.2272678.

Bryant, E.A., Haslett, S.K., 2007. Catastrophic wave erosion, Bristol Channel, United Kingdom: impact of tsunami? J. Geol. 115 (3), 253–269.

Calais, E., Symithe, S., Mercier de Lépinay, B., Prépetit, C., 2016. Plate boundary segmentation in the northeastern Caribbean from geodetic measurements and Neogene geological observations. Compt. Rendus Geosci. 348 (1), 42–51. https://doi.org/10.1016/j.crte.2015.10.007.

Calais, E., Symithe, S.J., de Lépinay, B.M., 2023. Strain Partitioning within the Caribbean–North America Transform Plate Boundary in Southern Haiti, Tectonic and Hazard Implications. Bull. Seismol. Soc. Am. 113 (1), 131–142. https://doi.org/10.1785/0120220121.

Corbeau, J., Rolandone, F., Leroy, S., Guerrier, K., Keir, D., Stuart, G., Clouard, V., Gallacher, R., Ulysse, S., Boisson, D., 2017. Crustal structure of western Hispaniola (Haiti) from a teleseismic receiver function study. Tectonophysics 709, 9–19.

Cotilla Rodríguez, M.O., 2011. ¿Tsunamis en Cuba? Física de La Tierra 23, 173–197. https://doi.org/10.5209/rev_fite.2011.v23.36918.

Cotilla Rodríguez, M.O., 2014. Sismicidad de interior de placa en Cuba. Rev. Geofís. 64, 93–125. https://doi.org/10.35424/regeofi.v0i64.312.

Cox, R., Jahn, K.L., Watkins, O.G., Cox, P., 2018. Extraordinary boulder transport by storm waves (west of Ireland, winter 2013–2014), and criteria for analysing coastal boulder deposits. Earth Sci. Rev. 177, 623–636.

Cox, R., Ardhuin, F., Dias, F., Autret, R., Beisiegel, N., Earlie, C.S., Herterich, J.G., Kennedy, A., Paris, R., Raby, A., Schmitt, P., Weiss, R., 2020. Systematic Review shows that work Done by storm Waves can be Misinterpreted as Tsunami-Related because Commonly used Hydrodynamic Equations are Flawed. Front. Mar. Sci. 7, 4. https://doi.org/10.3389/fmars.2020.00004.

Deepersonar, 2024. Deeper Sonar PRO+ 2. https://deepersonar.com.

DeMets, C., Jansma, P.E., Mattioli, G.S., Dixon, T.H., Farina, F., Bilham, R., Calais, E., Mann, P., 2000. GPS geodetic constraints on Caribbean-North America plate motion. Geophys. Res. Lett. 27 (3), 437–440.

Einstein, H.A., El-Samni, E.-S.A., 1949. Hydrodynamic forces on a rough wall. Rev. Mod. Phys. 21 (3), 520. https://doi.org/10.1103/RevModPhys.21.520.

Engel, M., May, S.M., 2012. Bonaire's boulder fields revisited: evidence for Holocene tsunami impact on the Leeward Antilles. Quat. Sci. Rev. 54, 126–141. https://doi.org/10.1016/j.quascirev.2011.12.011.

Etienne, S., Buckley, M., Paris, R., Nandasena, A.K., Clark, K., Strotz, L., Chagué-Goff, C., Goff, J., Richmond, B., 2011. The use of boulders for characterising past tsunamis: Lessons from the 2004 Indian Ocean and 2009 South Pacific tsunamis. Earth Sci. Rev. 107 (1–2), 76–90. https://doi.org/10.1016/j.earscirev.2010.12.006.

Fernández-Alvarez, J.C., Sorí, R., Pérez-Alarcón, A., Nieto, R., Gimeno, L., 2020. The role of tropical cyclones on the total precipitation in Cuba during the hurricane season from 1980 to 2016. Atmosphere 11 (11), 1–20. https://doi.org/10.3390/atmos11111156.

Frohlich, C., Hornbach, M.J., Taylor, F.W., Shen, C.-C., Moala, 'Apai, Morton, A.E., Kruger, J., 2009. Huge erratic boulders in Tonga deposited by a prehistoric tsunami. Geology 37 (2), 131–134.

Gandhi, D., Chavare, K.A., Prizomwala, S.P., Bhatt, N., Bhatt, N.Y., Mohan, K., Rastogi, B. K., 2017. Testing the numerical models for boulder transport through high energy marine wave event: an example from southern Saurashtra, western India. Quat. Int. 444, 209–216. https://doi.org/10.1016/j.quaint.2016.05.021.
Gienko, G.A., Terry, J.P., 2014. Three-dimensional modeling of coastal boulders using multi-view image measurements. Earth Surf. Process. Landf. 39 (7), 853–864. https://doi.org/10.1002/esp.3485.
Goto, K., Okada, K., Imamura, F., 2009. Characteristics and hydrodynamics of boulders transported by storm waves at Kudaka Island, Japan. Mar. Geol. 262 (1–4), 14–24. https://doi.org/10.1016/j.margeo.2009.03.001.
Goto, K., Miyagi, K., Kawamata, H., Imamura, F., 2010. Discrimination of boulders deposited by tsunamis and storm waves at Ishigaki Island, Japan. Mar. Geol. 269 (1–2), 34–45. https://doi.org/10.1016/j.margeo.2009.12.004.
Hall, A.M., Hansom, J.D., Williams, D.M., Jarvis, J., 2006. Distribution, geomorphology and lithofacies of cliff-top storm deposits: examples from the high-energy coasts of Scotland and Ireland. Mar. Geol. 232 (3–4), 131–155.
Hansom, J.D., Barltrop, N.D.P., Hall, A.M., 2008. Modelling the processes of cliff-top erosion and deposition under extreme storm waves. Mar. Geol. 253 (1–2), 36–50.
Hearty, P.J., Tormey, B.R., 2018. Listen to the whisper of the rocks, telling their ancient story. Proc. Natl. Acad. Sci. 115 (13), E2902–E2903. https://doi.org/10.1073/pnas.1721253115.
Imamura, F., Goto, K., Ohkubo, S., 2008. A numerical model for the transport of a boulder by tsunami. J. Geophys. Res. Oceans 113 (1), 1–12. https://doi.org/10.1029/2007JC004170.
INSMET, 2024. El Clima de Cuba. Características Generales. http://www.insmet.cu/asp/genesis.asp?TB0=PLANTILLAS&TB1=CLIMAC&TB2=/clima/ClimaCuba.htm.
Iturralde-Vinent, M., 2017. Huracanolitos, eventos de oleaje extremo y protección de las obras costeras. Revi. Anales de La Academ. de Ciencias de Cuba 7 (2), 4–10.
Iturralde-Vinent, M.A., García-Casco, A., Rojas-Agramonte, Y., Proenza, J.A., Murphy, J. B., Stern, R.J., 2016. The geology of Cuba: A brief overview and synthesis. GSA Today 26 (10), 4–10. https://doi.org/10.1130/GSATG296A.1.
James, M.R., Chandler, J.H., Eltner, A., Fraser, C., Miller, P.E., Mills, J.P., Noble, T., Robson, S., Lane, S.N., 2019. Guidelines on the use of structure-from-motion photogrammetry in geomorphic research. Earth Surf. Process. Landf. 44 (10), 2081–2084. https://doi.org/10.1002/esp.4637.
Kelletat, D., 2008. Comments to Dawson, AG and Stewart, I.(2007), Tsunami deposits in the geological record.—Sedimentary Geology 200, 166–183. Sediment. Geol. 211 (3–4), 87–91.
Kelletat, D., Schellmann, G., 2002. Tsunamis on Cyprus: field evidences and 14C dating results. Z. Geomorphol. 19–34.
Khalfaoui, O., Joudar, I., Chahid, N.E., El Khalidi, K., Minoubi, A., Bouchkara, M., Zourarah, B., 2024. The Safi boulders (Morocco): evidence of past extreme wave events. Mar. Geol. 470 (March), 107265. https://doi.org/10.1016/j.margeo.2024.107265.
Kirkgöz, M.S., 1986. Particle velocity prediction at the transformation point of plunging breakers. Coast. Eng. 10 (2), 139–147.
Lawrence, M.B., 2011. National Hurricane Center Tropical Cyclone Report: 2002-Hurricane Lili. https://www.nhc.noaa.gov/data/tcr/AL132002_Lili.pdf.
León-Brito, A.L., Hernández, R.-S., Pupo, Felipe-Matos, 2021. Huracanolitos en Trinidad. Condiciones naturales que favorecen su sedimentación. XIII Convención Internacional Sobre Medio Ambiente y Desarrollo. https://www.researchgate.net/publication/353555619_HURACANOLITOS_EN_TRINIDAD_CONDICIONES_NATURALES_QUE_FAVORECEN_SU_SEDIMENTACION.
Longuet-Higgins, M.S., 1952. On the statistical distribution of the heights of sea waves. J. Mar. Res. XI (3), 245–266.
Magaz, A.R., Portela, A.H., 2017. Huracanolitos: las huellas de tormentas colosales en las costas de Cuba. Cuba Geográfica 2 (5), 1–10.
Malavasi, S., Guadagnini, A., 2007. Interactions between a rectangular cylinder and a free-surface flow. J. Fluid. Structur. 23 (8), 1137–1148. https://doi.org/10.1016/j.jfluidstructs.2007.04.002.
Mann, P., Calais, E., Ruegg, J.-C., DeMets, C., Jansma, P.E., Mattioli, G.S., 2002. Oblique collision in the northeastern Caribbean from GPS measurements and geological observations. Tectonics 21 (6), 1–7.
Mastronuzzi, G., Sansò, P., 2000. Boulders transport by catastrophic waves along the Ionian coast of Apulia (southern Italy). Mar. Geol. 170 (1–2), 93–103.
Mastronuzzi, G., Pignatelli, C., Sansò, P., Selleri, G., 2007. Boulder accumulations produced by the 20th of February, 1743 tsunami along the coast of southeastern Salento (Apulia region, Italy). Mar. Geol. 242 (1–3), 191–205. https://doi.org/10.1016/j.margeo.2006.10.025.
Matos-Pupo, F., Peros, M., Rodríguez-Cueto, Y., Hernánde-Fernández, L., Guash-Hechavarría, F., 2018. Depósitos de huracanolitos en Jardines de la Reina (Cuba) provocados por oleajes extremos: paleohuracanes o paleotsunamis. XI Congreso de Ciencias Del Mar, MarCuba, p. 2018.
Matos-Pupo, F., León-Brito, A., Seco-Hernández, R., 2023. Distribución espacial de huracanolitos en las costas de Cuba. Minería y Geol. 39 (1), 1–14.
Matsukura, Y., Maekado, A., Aoki, H., Kogure, T., Kitano, Y., 2007. Surface lowering rates of uplifted limestone terraces estimated from the height of pedestals on a subtropical island of Japan. Earth Surf. Process. Landf. 32 (7), 1110–1115. https://doi.org/10.1002/esp.1510.
May, S.M., Willershäuser, T., Vött, A., 2010. Boulder transport by high-energy wave events at Cap Bon (NE Tunisia). Coastline Report. 16, 1–10.
May, S.M., Brill, D., Engel, M., Scheffers, A., Pint, A., Opitz, S., Wennrich, V., Squire, P., Kelletat, D., Brückner, H., 2015. Traces of historical tropical cyclones and tsunamis in the Ashburton Delta (north-West Australia). Sedimentology 62 (6), 1546–1572. https://doi.org/10.1111/sed.12192.
McDonald, W.F., 1935. The hurricane of august 31 to september 6, 1935. Mon. Weather Rev. 68 (9), 269–271.
Moore, J.G., Moore, G.W., 1984. Deposit from a giant wave on the island of Lanai, Hawaii. Science 226 (4680), 1312–1315.
Morton, R.A., Richmond, B.M., Jaffe, B.E., Gelfenbaum, G., 2006. Reconnaissance Investigation of Caribbean Extreme Wave Deposits - Preliminary Observations, Interpretations, and Research Directions. Open-File Report. U. S Geological Survey.
Morton, R.A., Richmond, B.M., Jaffe, B.E., Gelfenbaum, G., 2008. Coarse-clast ridge complexes of the Caribbean: a preliminary basis for distinguishing tsunami and storm-wave origins. J. Sediment. Res. 78 (9), 624–637.
Mottershead, D., Bray, M., Soar, P., Farres, P.J., 2014. Extreme wave events in the Central Mediterranean: Geomorphic evidence of tsunami on the Maltese Islands. Z. Geomorphol. 58 (3), 385–411. https://doi.org/10.1127/0372-8854/2014/0129.
Nagle-McNaughton, T., Cox, R., 2019. Measuring Change using Quantitative Differencing of repeat Structure-From-Motion Photogrammetry: the effect of Storms on Coastal Boulder Deposits. Remote Sens. 12 (1), 42. https://doi.org/10.3390/rs12010042.
Nandasena, N.A.K., 2017. Revisiting dimensionless coefficients of boulder transport equations: A small-scale experimental investigation on coefficient of lift. In: Proceedings of 5th International Tsunami Field Symposium. Presented at the Tsunami Field Symposium.
Nandasena, N.A.K., 2020. Chapter 29 - Perspective of incipient motion formulas: Boulder transport by high-energy waves. In: Geological Records of Tsunamis and Other Extreme Waves. Elsevier, pp. 641–659. https://doi.org/10.1016/B978-0-12-815686-5.00029-8.
Nandasena, N.A.K., Paris, R., Tanaka, N., 2011a. Numerical assessment of boulder transport by the 2004 Indian ocean tsunami in Lhok Nga, West Banda Aceh (Sumatra, Indonesia). Comput. Geosci. 37 (9), 1391–1399. https://doi.org/10.1016/j.cageo.2011.02.001.
Nandasena, N.A.K., Paris, R., Tanaka, N., 2011b. Reassessment of hydrodynamic equations: Minimum flow velocity to initiate boulder transport by high energy events (storms, tsunamis). Mar. Geol. 281 (1–4), 70–84. https://doi.org/10.1016/j.margeo.2011.02.005.
Nandasena, N.A.K., Tanaka, N., Sasaki, Y., Osada, M., 2013. Boulder transport by the 2011 Great East Japan tsunami: Comprehensive field observations and whither model predictions? Mar. Geol. 346, 292–309. https://doi.org/10.1016/j.margeo.2014.10.003.
Nandasena, N.A.K., Scicchitano, G., Scardino, G., Milella, M., Piscitelli, A., Mastronuzzi, G., 2022. Boulder displacements along rocky coasts: A new deterministic and theoretical approach to improve incipient motion formulas. Geomorphology 407, 108217. https://doi.org/10.1016/j.geomorph.2022.108217.
National Weather Service Forecast Office, 2002. Lili. Preliminary Storm Report. National Weather Service. https://web.archive.org/web/20030417141302/http://www.srh.noaa.gov/lch/tropical/lili/lili_psh.htm.
NOAA, 2022a. National Hurricane Center. NHC Data Archive. https://www.nhc.noaa.gov/data/#gis.
NOAA, 2022b. National Hurricane Center. 1995 Atlantic Hurricane Season. https://www.nhc.noaa.gov/data/tcr/index.php?season=1996&basin=atl.
NOAA Environmental Modeling Center, 2023. EMC Operational Wave Model Data Access. https://polar.ncep.noaa.gov/waves/download2.shtml.
NOAA Ocean Explorer, 2013. Comparing Hurricane Categories. https://oceanexplorer.noaa.gov/edu/learning/14_hurricanes/activities/hurricane_categories.html.
NOAA Tide Predictions, 2023. Annual Prediction Tide Tables for North Bimini, (TEC4617). https://tidesandcurrents.noaa.gov/noaatideannual.html?id=TEC4617.
Noormets, R., Crook, K.A.W., Felton, E.A., 2004. Sedimentology of rocky shorelines: 3.: Hydrodynamics of megaclast emplacement and transport on a shore platform, Oahu, Hawaii. Sediment. Geol. 172 (1–2), 41–65.
Nott, J., 1997. Extremely high-energy wave deposits inside the Great Barrier Reef, Australia: determining the cause-tsunami or tropical cyclone. Mar. Geol. 141 (1–4), 193–207. https://doi.org/10.1016/S0025-3227(97)00063-7.
Nott, J., 2003a. Tsunami or Storm Waves?:Determining the Origin of a Spectacular Field of Wave Emplaced Boulders Using Numerical Storm Surge and Wave Models and Hydrodynamic Transport Equations. J. Coast. Res. 19 (2), 348–356. http://www.jstor.org/stable/4299176.
Nott, J., 2003b. Waves, coastal boulder deposits and the importance of the pre-transport setting. Earth Planet. Sci. Lett. 210 (1–2), 269–276.
Núñez Jiménez, A., 1959. Geografía de Cuba. Editorial Lex, La Habana.
Núñez Jiménez, A., 1973. Geografía de Cuba. Pueblo y Educación, La Habana.
Núñez Jiménez, A., 1982. Cuba, La Naturaleza y el Hombre: Bojeo. Letras Cubanas, La Habana.
Paris, R., Fournier, J., Poizot, E., Etienne, S., Morin, J., Lavigne, F., Wassmer, P., 2010. Boulder and fine sediment transport and deposition by the 2004 tsunami in Lhok Nga (western Banda Aceh, Sumatra, Indonesia): A coupled offshore–onshore model. Mar. Geol. 268 (1–4), 43–54. https://doi.org/10.1016/j.margeo.2009.10.011.
Paris, R., Naylor, L.A., Stephenson, W.J., 2011. Boulders as a signature of storms on rock coasts. Mar. Geol. 283 (1–4), 1–11. https://doi.org/10.1016/j.margeo.2011.03.016.
Pasch, R.J., Lawrence, M.B., Avila, L.A., Beven, J.L., Franklin, J.L., Stewart, S.R., 2004. Atlantic hurricane season of 2002. Mon. Weather Rev. 132 (7), 1829–1859. https://doi.org/10.1175/1520-0493(2004)132<1829:AHSO>2.0.CO;2.
Pasch, R.J., Brown, D.P., Blake, E.S., 2011. Tropical Cyclone Report Hurricane Charley 9–14 August 2004. https://www.nhc.noaa.gov/data/tcr/AL032004_Charley.pdf.
Pedoja, K., Dunán-Avila, P., Jara-Muñoz, J., Authemayou, C., Nuñez-Labañino, A., de Gelder, G., Chauveau, D., Peñalver, L., Frometa, P.D.J.B., Martin-Izquierdo, D., Abella, E.C., Bertin, S., Rodríguez-Valdés, Á.R., Arango-Arias, E.D., Traoré, K., Regard, V., 2023b. On a ~210 t Caribbean coastal boulder: The huracanolito seaward of the ruins of the Bucanero resort, Juragua, Oriente, Cuba. Earth Surf. Process. Landf. 48 (15), 3074–3090. https://doi.org/10.1002/esp.5682.

Peñalver Hernández, L.L., Pérez Pérez, C.M., Cabrera Castellanos, M., 2009. Camellones de tormenta en Cuba. In: Su explotación local. XI I I Congreso Latinoamericano de Ciencias Del Mar, ColacMar La Habana, Cuba.
Peñalver, L., Cabrera, M., Delgado, R., Rodriguez, L., Pantaleon, G., Ugalde, C., Pérez, C., Denis, R., 2008. Mapa Digital de los Dep ositos Cuaternarios del Archipiélago Cubano a escala 1: 250.000. Instituto de Geología y Paleontología, La Habana.
Peñalver, L., Pedoja, K., Martin-Izquierdo, D., Authemayou, C., Nuñez, A., Chauveau, D., de Gelder, G., Davilan, P., Husson, L., 2021. The Cuban staircase sequences of coral reef and marine terraces: A forgotten masterpiece of the Caribbean geodynamical puzzle. Mar. Geol. 440 (July), 106575. https://doi.org/10.1016/j.margeo.2021.106575.
Pepe, F., Corradino, M., Parrino, N., Besio, G., Presti, V. Lo, Renda, P., Calcagnile, L., Quarta, G., Sulli, A., Antonioli, F., 2018. Boulder coastal deposits at Favignana Island rocky coast (Sicily, Italy): Litho-structural and hydrodynamic control. Geomorphology 303, 191–209. https://doi.org/10.1016/j.geomorph.2017.11.017.
Pignatelli, C., Sanso, P., Mastronuzzi, G., 2009. Evaluation of tsunami flooding using geomorphologic evidence. Mar. Geol. 260 (1–4), 6–18.
Raichlen, F., 2012. Waves. The MIT Press.
Regnauld, H., Oszwald, J., Planchon, O., Pignatelli, C., Piscitelli, A., Mastronuzzi, G., Audevard, A., 2010. Polygenetic (tsunami and storm) deposits? A case study from Ushant Island, western France. Zeitschrift Für Geomorphol. Supplemen. Issu. 197–217. https://hdl.handle.net/11586/79761.
Reguero, B.G., Méndez, F.J., Losada, I.J., 2013. Variability of multivariate wave climate in Latin America and the Caribbean. Glob. Planet. Chang. 100, 70–84. https://doi.org/10.1016/j.gloplacha.2012.09.005.
Rodríguez-Valdés, Á.R., Acosta-Rodríguez, E., 2017. Megabloques en Trinidad : Generalidades de su morfometría. Serie Oceanol. 16, 1–7. http://hdl.handle.net/1834/12944.
Rojas-Consuegra, R., Isaac-Mengana, J., 2007. Depósitos detríticos gruesos producidos por el huracán Wilma, sobre la costa este de Ciudad de la Habana. Memorias, Trabajos y Resúmenes. II Convención Cubana de Ciencias de La Tierra (Geociencias' 2007). Centro Nacional de Información Geológica. Instituto de Geología y Paleontología de Cuba, La Habana, CD-Rom.
Rojas-Consuegra, R., Isaac-Mengana, J., 2008. Depósitos sedimentarios raros del huracán Wilma en la costa habanera: Influencia antropogénica. In: Convención Trópico 2008: III Congreso de Geografía Tropical. Trabajos. La Habana, pp. 1–13. https://www.researchgate.net/profile/Reinaldo-Consuegra/publication/279530714_DEPOSITOS_SEDIMENTARIOS_RAROS_DEL_HURACAN_WILMA_EN_LA_COSTA_HABANERA_INFLUENCIA_ANTROPOGENICA/links/55955f7308ae5d8f3930eeba/DEPOSITOS-SEDIMENTARIOS-RAROS-DEL-HURACAN-WILMA-EN-L.
Rojas-Consuegra, R., Isaac-Mengana, J., Pupo, F.M., Peros, M.C., 2019. Coarse Detrital Deposits from Hurricane Wilma on the Western Coast of Cojimar, Havana, Cuba. In: Cárdenas, R., Mochalov, V., Parra, O., Martin, O. (Eds.), Proceedings of the 2nd International Conference on BioGeoSciences. Springer International Publishing, pp. 111–125. https://doi.org/10.1007/978-3-030-04233-2_10.
Roura-Pérez, P., Sistachs-Vega, V., Vega, R., AlpizarTtirzo, M., 2018. Climatic statistical characterization of hurricanes in Cuba during the period 1791-2016. Revi. Cubana de Meteorol. 24 (3), 304–312. http://opn.to/a/kzMxk.
Rovere, A., Casella, E., Harris, D.L., Lorscheid, T., Nandasena, N.A.K., Dyer, B., Sandstrom, M.R., Stocchi, P., D'Andrea, W.J., Raymo, M.E., 2017. Giant boulders and last Interglacial storm intensity in the North Atlantic. Proc. Natl. Acad. Sci. 114 (46), 12144–12149. https://doi.org/10.1073/pnas.1712433114.
Rubin, K.H., Fletcher III, C.H., Sherman, C., 2000. Fossiliferous Lana'i deposits formed by multiple events rather than a single giant tsunami. Nature 408 (6813), 675–681.
Salzmann, L., Green, A., 2012. Boulder emplacement on a tectonically stable, wave-dominated coastline, Mission Rocks, northern KwaZulu-Natal, South Africa. Mar. Geol. 323, 95–106.
Scheffers, A., Kelletat, D., 2003. Sedimentologic and geomorphologic tsunami imprints worldwide—a review. Earth Sci. Rev. 63 (1–2), 83–92.
Scheffers, A., Kelletat, D., 2006. New evidence and datings of Holocene paleo-Tsunami events in the Caribbean (Barbados, St. Martin and Anguilla). In: Caribbean Tsunami Hazard, pp. 178–202. https://doi.org/10.1142/9789812774613_0008.
Scheffers, S., Scheffers, A., Kelletat, D., Bryant, E.A., 2008. The Holocene paleo-tsunami history of West Australia. Earth Planet. Sci. Lett. 270 (1–2), 137–146.
Schneider, B., Hoffmann, G., Falkenroth, M., Grade, J., 2019. Tsunami and storm sediments in Oman: Characterizing extreme wave deposits using terrestrial laser scanning. J. Coast. Conserv. 23 (4), 801–815. https://doi.org/10.1007/s11852-018-0663-4.
Scicchitano, G., Monaco, C., Tortorici, L., 2007. Large boulder deposits by tsunami waves along the Ionian coast of South-Eastern Sicily (Italy). Mar. Geol. 238 (1–4), 75–91. https://doi.org/10.1016/j.margeo.2006.12.005.
Scicchitano, G., Scardino, G., Tarascio, S., Monaco, C., Barracane, G., Locuratolo, G., Milella, M., Piscitelli, A., Mazza, G., Mastronuzzi, G., 2020. The first Video Witness of Coastal Boulder Displacements Recorded during the Impact of Medicane "Zorbas" on Southeastern Sicily. Water 12 (5), 1497. https://doi.org/10.3390/w12051497.
Scicchitano, G., Scardino, G., Monaco, C., Piscitelli, A., Milella, M., De Giosa, F., Mastronuzzi, G., 2021. Comparing impact effects of common storms and Medicanes along the coast of South-Eastern Sicily. Mar. Geol. 439, 106556. https://doi.org/10.1016/j.margeo.2021.106556.
Sedrati, M., Morales, J.A., El M'rini, A., Anthony, E.J., Bulot, G., Le Gall, R., Tadibaght, A., 2022. Using UAV and Structure-From-Motion Photogrammetry for the Detection of Boulder Movement by Storms on a Rocky Shore Platform in Laghdira, Northwest Morocco. Remote Sens. 14 (16), 4102. https://doi.org/10.3390/rs14164102.
Servicio Hidrográfico y Geodésico de la República de Cuba, 2003. Derrotero de las costas de Cuba. GEOCUBA and EDIMAR, Agencia de Cartografía Náutica.
Shah-Hosseini, M., Saleem, A., Mahmoud, A.-M.A., Morhange, C., 2016. Coastal boulder deposits attesting to large wave impacts on the Mediterranean coast of Egypt. Nat. Hazards 83, 849–865.
Simpson, R.H., 1974. The hurricane disaster—potential scale. Weatherwise 27 (4), 169–186.
Sleath, J.F.A., 1984. Sea Bed Mechanics.
Stewart, S.R., 2017. National Hurricane Center Tropical Cyclone Report: Hurricane Matthew (AL142016). In: National Hurricane Center. http://www.nhc.noaa.gov/data/tcr/AL142016_Matthew.pdf.
Suanez, S., Fichaut, B., Magne, R., 2009. Cliff-top storm deposits on Banneg Island, Brittany, France: Effects of giant waves in the Eastern Atlantic Ocean. Sediment. Geol. 220 (1–2), 12–28. https://doi.org/10.1016/j.sedgeo.2009.06.004.
Sunamura, T., 1992. Geomorphology of Rocky Coasts (Volumen 3). Wiley. https://books.google.fr/books?id=vF7uAAAAMAAJ.
Switzer, A.D., Burston, J.M., 2010. Competing mechanisms for boulder deposition on the southeast Australian coast. Geomorphology 114 (1–2), 42–54. https://doi.org/10.1016/j.geomorph.2009.02.009.
Terry, J.P., Lau, A.Y.A., Etienne, S., 2013. Reef-Platform Coral Boulders - evidence for High-Energy Marine Inundation events on Tropical Coastlines. In: In Reef-Platform Coral Boulders (Issue 2011). Springer, Singapore. https://doi.org/10.1007/978-981-4451-33-8.
Terry, J.P., Dunne, K., Jankaew, K., 2016. Prehistorical frequency of high-energy marine inundation events driven by typhoons in the Bay of Bangkok (Thailand), interpreted from coastal carbonate boulders. Earth Surf. Process. Landf. 41 (4), 553–562.
Williams, D.M., Hall, A.M., 2004. Cliff-top megaclast deposits of Ireland, a record of extreme waves in the North Atlantic—storms or tsunamis? Mar. Geol. 206 (1–4), 101–117. https://doi.org/10.1016/j.margeo.2004.02.002.
Young, R.W., Bryant, E.A., Price, D.M., 1996. Catastrophic Wave (Tsunami?) Transport of Boulders in southern New South Wales, Australia. https://ro.uow.edu.au/scipapers/91.
Yu, K., Zhao, J., Roff, G., Lybolt, M., Feng, Y., Clark, T., Li, S., 2012. High-precision U-series ages of transported coral blocks on Heron Reef (southern Great Barrier Reef) and storm activity during the past century. Palaeogeogr. Palaeoclimatol. Palaeoecol. 337, 23–36.